Hydrothermal fracking of geothermal wells

Author: K. Ritsema & N. Buik (IF Technology)

COOPERATING COMPANIES & UNIVERSITIES

GEOCAP
Geothermal Capacity Building Program Indonesia - Netherlands

INAGA

University of Twente, Faculty ITC

IF technology

University of Indonesia

DNV GL

Gadjah Mada University

Technical University Bandung

Utrecht University, Faculty of Geosciences, Department of Earth Sciences

Delft University of Technology, Department of Geotechnology

Netherlands Organisation for Applied Scientific Research

TABLE OF CONTENTS

1 INTRODUCTION

1.1 CONTEXT AND BACKGROUND

IF Technology is, together with several companies and research institutes in the Netherlands, partner in the international program GEOCAP (https://www.geocap.nl/). GEOCAP – the Geothermal Capacity Building Program – is a collaboration between the Dutch and Indonesian entities aiming to improve the production of geothermal energy in Indonesia. Due to the abundance of high enthalpy formations – rock formations at high temperature conditions –, the geothermal potential of Indonesia is estimated to be one of the largest in the world. It is often referred to as the 'sleeping giant' in terms of geothermal energy development. However the country itself does not have sufficient skilled personnel to realize production and therefore GEOCAP aims to develop geothermal programmes for education and training, research and subsurface databases. This report contributes to work package 2.05 of GEOCAP. This package focuses on hydro-fracking and acidizing and concerns reservoir stimulation and its practice in enhancing the productivity of geothermal wells.

Since drilling is the largest expense in geothermal energy projects, lowering these costs would lead to a substantial increase in the economy of a geothermal project. Reservoir stimulation helps to increase well production or injectivity by increasing the permeability and conductivity of the rock around the well. Currently, there are three types of reservoir stimulation techniques: hydraulic stimulation, geochemical stimulation and thermal stimulation. Hydraulic stimulation uses high pressured fluid injection to overcome the shear strength of the fracture network and enhances permeability around the well, chemical stimulation is used to dissolve the rock material and fracture walls to increase permeability and thermal stimulation uses the temperature differential between the cold injection fluid and the hot reservoir to induce a thermal shock by instantaneously cooling the rock around the well, which lowers the effective shear strength of the rock creating and opening-up fractures.

Which stimulation technique is best to be used depends highly on the site-specific parameters, such as the geological setting, rock types and properties, the state of stress in the reservoir and the history of the well. Though, a literature study by Van den Broek (2015, report of IF Technology) has pointed out that thermal stimulation has the highest success rate of the three stimulation techniques in high enthalpy reservoirs: however it is not yet widely used.
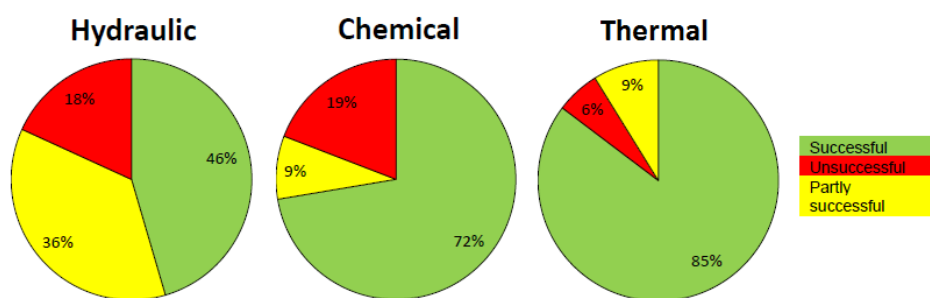
Figure 1: *Pie charts showing the success rate of the various stimulation techniques. Note that not all techniques are used as frequently. (Van den Broek, 2015)*

1.2 OBJECTIVES AND APPROACH

A semi-analytical model was developed that provides insight in the effectiveness of thermal stimulation techniques in particular fields. The aim of the model is to contribute as a quick scan tool for operators to get a first order approximation if thermal stimulation can acquire the desired permeability enhancement for stimulation treatments. The model incorporates poro-elastic and thermo-elastic stress changes due to cold fluid injection around the injector and solves the criterion for fracture formation. As soon as a fracture is initiated it starts to grow away from the well, lowering the skin of the well and decreasing the fluid pressure in the bore hole. Lowering the skin subsequently results in an increase in injectivity and productivity of the well, as fluid can flow more easily into the reservoir with lower injection pressure.

2 RESERVOIR STIMULATION

2.1 GEOTHERMAL ENERGY SYSTEMS

Sustainable energy in the Netherlands can successfully be produced from heat resources in shallow sub-surface systems, also referred to as geothermal doublets. A geothermal Doublet is the technical method that is used to extract geothermal energy from the subsurface by injection fluid through an injection well and extracting hot water from a production well (Fig. 1). Temperatures ranging between 40 °C and 120 °C can be directly used for the heating of greenhouses or residential houses. In the Dutch subsurface these temperatures are observed between 1000 till 3500 meter and can generate 5 MW or more (ThermoGIS.nl).
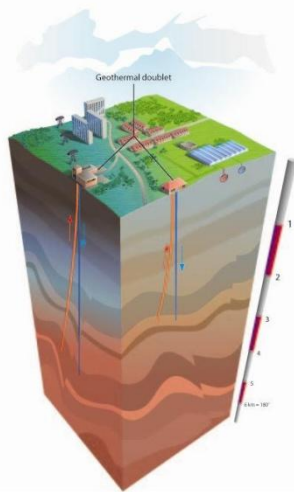
A heat exchanger at the surface extracts the heat from the produced water which cools down again when it is used for heating. The cooled water is thereafter re-injected into the reservoir through the injection well. This re-injection of water is essential since it keeps the stress changes at depth to a minimum and reduces the risks on earthquakes or reservoir subsidence.

An efficient geothermal system for energy production has to meet some requirements. First, the reservoir needs to have sufficient porosity and permeability. The porosity measures the percentage of pores that are present in a reservoir and determines the volume of water that a reservoir can hold. The permeability defines how those pores are interconnected and the higher the permeability the better the fluid pathways within the reservoir are. This is essential to maintain sufficient fluid flow from the injector to the producer in a doublet system.

Figure 2: Schematic overview of a geothermal doublet. Cold water is injected through an injection well (blue) and hot water is extracted from a production well (orange) At the surface a heat exchanger extracts the heat from the water, which can be used for heating and electricity. (www.ThermoGIS.nl)

Thereby, the reservoir rock should have a high temperature, as the higher the temperature of the produced fluids, the higher the energy potential of the system. Temperatures vary per geological setting and depth of a reservoir. And last, the reservoir should be as homogeneous as possible, since heterogeneous zones will affect the fluid flow and may decrease the produced power. Natural barriers, such as faults for instance, can be sealing and may prevent fluids to flow through.

During injection fluids migrate into the reservoir around the well. This produces a flooded front and a cooled front, respectively the area around the well that increases in pressure due to fluid injection and an area that decreases in temperature due to the temperature differential of the injection fluid and the reservoir. Generally, the flooded front is larger than the cooled front, since fluid transport is faster than temperature transport (Perkins, 1985). The lifetime of a geothermal doublet is highly dependent on the extent of the temperature front, considering that the energy potential decreases as soon as the cooled front reaches the production well.

The distribution of pressure and temperature also has other side-effects, since they affect the stress and strain field within the reservoir and the surrounding rock mass. As explained more elaborately in the following sections, this can have positive and negative effects. Injection can result in hydrothermal fracturing of the reservoir. This enhances the permeability and fluid flow through the reservoir and increases the productivity of the doublet. On the other hand, hydrothermal processes may increase

the risk on induced seismicity associated with injection or can result in reservoir compaction and subsequent surface subsidence.

2.2 HYDROTHERMAL STIMULATION

The operation of geothermal doublets requires a significant amount of energy. The injection and production pumps have to overcome the flow resistance of the reservoir in order to maintain sufficient fluid flow throughout the system. Flow resistance of a reservoir is highly dependent on properties of the reservoir and fluids. Fluid properties, such as density, viscosity and heat capacity vary with pressure and temperature (Adams, 2002; Batzle, 1992; Sun, 2008), which affects the ability to flow. On the other hand, reservoir properties as porosity and permeability also affect the flow capacity, since low porosity and permeability reservoirs do not accommodate sufficient fluid migration pathways to accompany fluid transport. Enhancing the permeability of a reservoir, and therefore improving the productivity of your geothermal system, is possible by the use of reservoir stimulation techniques. The three main stimulation techniques are chemical stimulation, hydraulic stimulation and thermal stimulation. So far, these techniques have been widely developed in the hydrocarbon industry, however applying then to high temperature geothermal systems involves different processes as reservoir temperatures are generally much higher in these systems than in hydrocarbon reservoirs (Van den Broek, 2015). This affects the reservoir and flow properties.
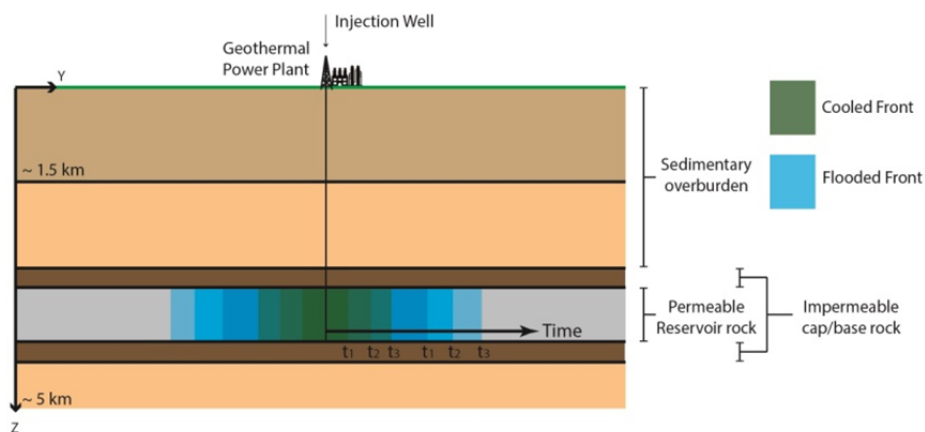
Figure 3: *Schematic side view of a geothermal well. Relatively cold fluids are injected into a hot reservoir. This results in a propagating fluid and cooled front, which are both increasing in time ($t_1 < t_2 < t_3$) . The cap and base rock are assumed to have an infinite thickness and to be impermeable. No fluid flows across, however heat transport may.*

This study focuses on hydrothermal stimulation of low and high enthalpy geothermal systems. This technique includes the formation of fractures around the well as a result of the combination of injection pressure and the temperature differential between the hot reservoir and the injection fluid (Fjaer, 2008; Economides, 2000). The process can also cause opening of natural fractures that are already present in the rock formation (Ge, 2009).

2.2.1 INDUCED STRESS CHANGE IN SUBSURFACE RESERVOIRS

The injection of fluids into a subsurface reservoir changes the in situ stress state of the reservoir system in several ways; (1) poro-mechanical effects caused by changes in the pore fluid pressure of the reservoir, (2) thermal effects caused by changing the pore fluid temperature and (3) chemical effects due to changes in the pore fluid chemistry and buoyancy effects due to changes in pore fluid density (Orlic, 2011; Veldkamp, 2015). These effects combined can result in damage to the area in the vicinity of the wellbore.

Poro-elasticity

By nature, subsurface rocks are filled with cracks and pores that are saturated with one or more fluid phases, such as water for geothermal reservoirs and oil or gas for hydrocarbon reservoirs. When a fluid, whether similar to the original formation fluid or not, is injected into a geologic formation, it changes the pore pressure. This causes deformation processes and changes in the total stress within the reservoir and its surroundings due to the coupling between pore pressure and stress (Altmann, 2010).

In porous media fluids leak-off into the formation and this induces pore pressure build ups away from the injection well and results in a dilation of the surrounding rock by changing its volume. This is explained by the theory of poro-elasticity. Assuming uniaxial strain in the vertical direction in an isotropic and linear elastic reservoir, the minimum horizontal stress can be calculated by Eaton's theory that defines σ_h by a relationship between the overburden stress, the pore pressure in the reservoir, the Poisson's ratio of the rock and Biot's coefficient (Eq. 3).

(1) $\sigma_v = \rho_l g z$

(2) $P_{res} = \rho_w g z$

(3) $\sigma_h = \left(\dfrac{\nu}{1-\nu}\right)(\sigma_v - \alpha P_{res}) + \alpha P_{res}$

(4) $\alpha = 1 - \dfrac{K_{fr}}{K_s}$

With symbols being:

σ_v = Vertical stress [Pa]
σ_h = Minimum horizontal stress [Pa]
P_{res} = Reservoir pressure [Pa]
ν = Poisson's ratio [-]
g = Gravitational acceleration [9.81 m/s^2]
z = Reservoir depth [m]
ρ = Density [kg/m^3]
α = Biot's coefficient [-]

The Biot's coefficient is defined in equation 4, in which K_{fr} is the drained bulk modulus of the reservoir [Pa] and K_s is the bulk modulus of the solid rock [Pa] (Fjaer, 2008). This indicates the amount of rock consolidation and can therefore tell whether poro-elastic effects can be expected (Biot, 1941). Most geomechanical studies assume a Biot's coefficient of $\alpha = 1$. This implies that $K_{fr} << K_s$, meaning that the rock is highly porous and weakly consolidated. A Biot's coefficient near 0, $K_{fr} = K_s$, on the other hand, means that the rock is nearly solid and has a low porosity and permeability, e.g. not many migration pathways for fluids to flow. Rocks that have a Biot's value smaller than 1, are therefore less affected by changes in the pore pressure. In geothermal systems, fluids are often injected in highly permeable sedimentary basins where a Biot's value close to 1 is applicable. For instance, a Biot's value of 0.8 is often accepted for sandstones (Zoback, 2007). However, geothermal systems are also developed in areas that are still seismically active and the reservoir rock is probably more consolidated. For those hard rock reservoirs a Biot's value of $0.5 < \alpha < 1$ can be expected (Brouwer, 2005).

As can be derived from equation 3, an increase in pore pressure affects the minimum horizontal stress. The relationship between the change in horizontal stress ($\Delta\sigma_h^P$) and the change in pore fluid pressure (ΔP) can be defined as follows (Fjaer, 2008; Zoback, 2007; Hassanzadegan, 2011):

(5) $\Delta\sigma_h^P = \dfrac{1-2\nu}{1-\nu}\alpha\Delta P$

On one side, an increase in pore pressure thus leads to an increase of the horizontal stress within this region (Economides (2010) p. , Orlic (2005)). However, on the other hand the change in pore pressure also directly decreases the effective horizontal stress. The effective stress can be simply calculated by subtracting the total pore pressure from the total stress; $\sigma'_h = \sigma_h - \alpha P_{res}$. The total stress changes due to poro-elastic effects can therefore be described by the so called stress path ratio (Eq. 6) and is for extensional regimes generally in the range of 0.5-0.7 (Zoback, 2007) and for compression regimes in the order of 1.5.

$$(6) \quad \frac{\Delta\sigma_h^P}{\Delta P} = \frac{\Delta\sigma_H^P}{\Delta P} = \gamma_h^P = \frac{1-2v}{1-v}\alpha$$

The vertical stress in the reservoir is assumed to be unaffected by the pore pressure change and is therefore constant through time and has the value of the overburden (Van Wees, 2014; TNO, 2014). Note though, that the effective vertical stress does change proportional to the stress change.

Thermo-elasticity

Studies often assume isothermal conditions in geomechanical analyses (Rutqvist, 2008; Suri, 2010; Altmann, 2010; Wang, 2016), however, thermal effects may under certain circumstances have a major effect on the stress changes. In the case of geothermal energy, relatively cold water is injected into a relatively hot reservoir. This causes cooling of the rock formations around the injection well. As a result, thermal stresses are induced not only in the cooled area by contraction, but also in the surrounding rock formations by extension. Similar to the pore pressure, these temperature changes also affect the effective horizontal stresses, also referred to as themo-elasticity. Although, there are still disagreements in how to calculate this term, the following equation gives the most common expression as stated by (Zoback, 2007).

$$(7) \quad \Delta\sigma_h^T = \frac{E\beta\Delta T}{1-v}$$

In which E is the Young's modulus [Pa], β is the linear expansion coefficient of the reservoir rock [°C^{-1}] and is mostly in the order of 1e-5 for sandstone reservoirs (Zoback, 2007; TNO, 2014) and ΔT is the temperature drop and is negative for cooling. The thermal stress drop is thus negative and can be simply added to the linear elasticity equations. Whether this drop is significant or not depends on some essential factors; the thermal properties of the injective and the reservoir rock, the temperature differential, the flow characteristics, injection rate and volume and he type of fluids that are injected. Fluids can have different properties, such as heat capacity and thermal conductivity. Equation 7 shows that stress reduction due to thermal effects can be of major importance in 1) stiff reservoirs, 2) formation with large thermal expansion coefficients and 3) with large temperature differences. The latter is largely applicable to (enhanced) geothermal systems.

Chemical effects

The chemical character of any water depends on the original water composition and the rock mineralogy, and is the product of time-dependent processes, such as rock-water interactions and transport processes as diffusion, dispersion, mixing and convection. According to literature (Adams, 2002; Batzle, 1992; Sun, 2008) the physical properties of formation waters in sedimentary basins can vary as a result of temperature (T), pressure (P) and total dissolved solutes (TDS), also referred to as salinity. The most important parameters that are affected by P, T and TDS are the density, viscosity and heat capacity of fluids.

The flow rate and injectivity of a well depend on the permeability of the formation and the flow capability of the fluid. Therefore, variations in the viscosity and density of brine fluids can have a significant effect on the flow pattern in a sedimentary basin. Density differences may enhance or retard flow driven by injection and can initiate buoyancy driven flow. To properly predict the effectiveness of fluid injection we therefore have to include estimates of the formation water properties at in situ condition and changed properties as a result of perturbation. The most important changes around a geothermal well are:

- The friction in the injection well increases due to a higher fluid viscosity. This increases the required injection pump pressure (Veldkamp, 2015).
- The density of cold water is higher and therefore the water column in the injection well becomes heavier. Therefore less injection pump pressure is required.

- Cold water is less easily injected into a subsurface reservoir by an increase in inflow resistance. This increases the injection pump pressure.
- The heat capacity of cold water is lower than for hot water. More energy is needed to heat up the cold fluid front again after injection is terminated.

Note that these chemical effects of formation brines should not be confused with chemical stimulation of geothermal fields, which includes the addition of acids to the injective to enhance permeability of the reservoir.

2.2.2 FRACTURE MECHANICS; INITIATION AND GROWTH

The goal of a hydrothermal stimulation job is to create fractures around the injection wellbore that increase the permeability and connectivity of your reservoir. During hydrothermal stimulation water in injected until the induced stresses at the borehole wall are large enough to cause a fracture to open and propagate into the formation (Jaeger, 2007). This condition is met when the injection pressure exceeds the sum of the minimum principal stress (σ_3) and the tensile strength of the rock (σ_{ten}). The pressure needed to initiate failure is also referred to as the breakdown pressure.

Fractures are formed in the mode I approximation, the opening mode, where the fracture opens in the direction of the least principal stress (Fig. 3). The fracture criterion for tensile failure is described as follows (Perkins, 1985; Koning, 1988; Van den Broek, 2015):

$$(8) \quad P_{BH} \geq \sigma_3 + \sigma_{ten} + \Delta\sigma_3^T + \Delta\sigma_3^P$$

In which P_{BH} is the borehole pressure [Pa], σ_3 is the least principal stress [Pa], $\Delta\sigma_3^T$ and $\Delta\sigma_3^P$ are the stress changes due to temperature and pressure, where $\Delta\sigma_3^T$ is negative for cold fluid injection and $\Delta\sigma_3^P$ is positive. σ_{ten} is the tensile strength of the rock and is assumed to be zero, as the tensile rock strength in already fractured reservoirs is negligible.
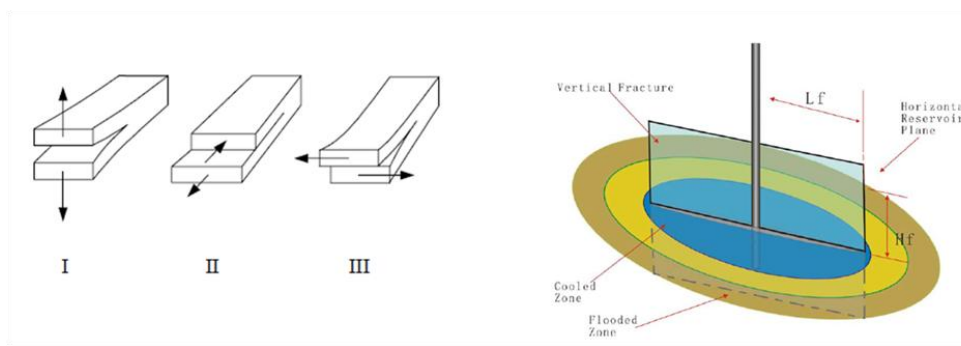

Figure 4: Left) Schematic sketch of three fundamental modes of failure. Right) Plan view of a two-winged hydraulic fracture (Ge, 2009).

Generally, in (deep) geological formations, the vertical stress is a result of the overburden pressure (σ_v). Then, the two other principal stresses (σ_2 and σ_3), are oriented in the horizontal plane and are also referred to as the maximum horizontal stress (σ_H) and the minimum horizontal stress (σ_h). Hydraulically-driven fractures are considered to grow in the Mode I, or opening mode (**Figure 4**). The displacement of the fracture walls is perpendicular to the plane of the fracture, in other words in the direction of the minimum principal stress. In sedimentary basins this is generally the minimum horizontal stress σ_h, which implies either a strike-slip or normal stress regime. In that case the fracture propagates in the direction of the maximum horizontal stress σ_H and is vertical.

Off course, it is also possible that the vertical stress is the smallest principal stress. This may be the case in areas of extensive tectonic activity, areas which have been uplifted without the release of the horizontal stress or at shallow depths in the subsurface (Fjaer, 2008). The fracture will then extend horizontally.
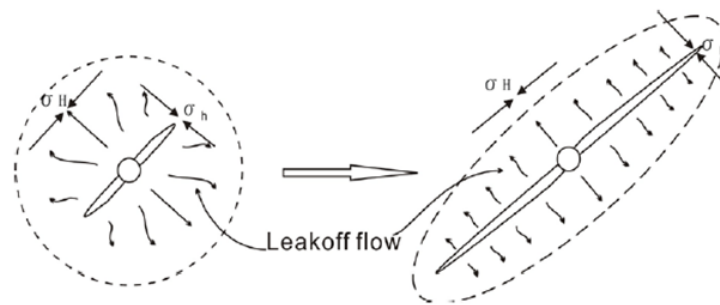
Figure 5: *Flow system evolution (Ge, 2009). The leak-off changes from a radial distribution prior to fracture formation, or for really small fractures, to elliptical for growing fractures.*

If the injection is as such that hydraulic fractures are created, the flow system around the fracture will evolve from an initially radial geometry to an elliptical geometry (**Figure 5**). These elliptical shapes become flatter while the fracture is growing. The criterion for fracture propagation is more complex than the criterion for fracture initiation, as it also has to account for fluid flow and fluid loss due to fracture formation.

The net pressure at the fracture tip should always be zero, and is defined by subtracting the tensile strength of the rock at the tip of the fracture from the pressure at the fracture tip. As soon as the pore pressure overcomes the tensile strength, i.e. the net pressure is positive, and the fracture propagates as such that the net pressure at the tip becomes zero again. This is similar to fracture initiation. However, how the pressure at the fracture tip evolves during injection depends on the loss of fluid to the formation, i.e. the distribution of the temperature and pressure changes around the fracture, and the evolution of fluid flow from the well bore to the fracture tip. According to previous studies by (Ge, 2009), the critical factors that affect fracture propagation include;

- The in situ stress conditions in the reservoir: The local stress fields and orientations determine the fracture orientation and fracture growth rate.
- The thickness of the pay zone: The total thickness of the formation in the vicinity of the well affects the fracture length.
- Mechanical rock properties: such as the Young's modulus, Poisson's ratio and the thermal expansion coefficient will affect fracture propagation.
- Fluid pressure gradients in the fracture: the fluid pressure in the borehole is not the same as the fluid pressure at the fracture tip due to fracture roughness and leak-off.
- Pore pressure and temperature distribution: The P&T distribution around the fracture changes from a radial pattern to elliptical.

Fracture Propagation models

Many models have been developed in the past to study fracture propagation. The most traditional 2D models are; the PKN model, the KGD, and the radial model (Error! Reference source not found.). These models were originally based on fracture propagation driven by fluid flow and did not account for any thermal effects. The models are capable of calculating the fracture geometry, including the width, fracture length and flow rate within the fracture. A brief overview of the various aspects of the models is given in shown in Table 1.
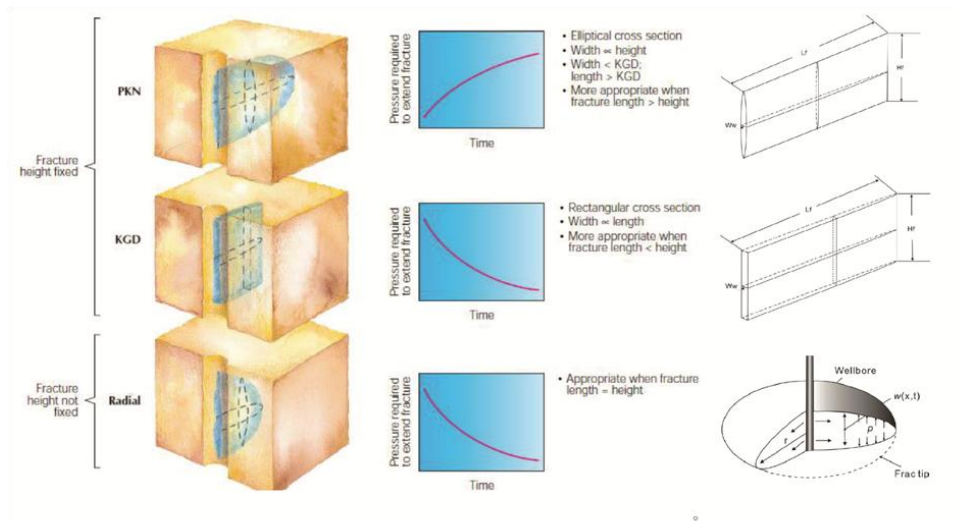
Figure 6 Characteristics of the three general fracture propagation models; PKN, KGD and Radial. Modified after (Brady, 1992), (Ge, 2009) and (Pizzocolo, 2016).

The PKN model was first introduced by (Perkins T. K., 1961) and was later improved by (Nordgren, 1972), who added fluid leak off and storage to the equation. They assumed a vertical fracture that propagates through a fully confined reservoir has a fixed height, which is the same size as the thickness of the reservoir. The stresses in the over- and underlying layers are assumed to be sufficiently large to prevent the fracture from growing out of the pay zone. The fracture has an elliptical cross section in both the horizontal and vertical plane and reaches its maximum width at the wellbore (**Figure 5**). The problem is solved in 2D by using the plane strain assumption. Plain strain is assumed in the vertical direction and implies that elastic deformation is fully concentrated in the vertical planes perpendicular to the direction of fracture propagation (Ge, 2009). This is equivalent to assuming that the pressure at any section is dominated by the height of the section, rather than the length of the fracture (Economides, 2000). This is true if the fracture length is much larger than the height.

The KGD model is also named after its developers (Kristianovitch, 1955) and (Geertsma J. d., 1969). It is similar to the PKN model, as it is also only applicable to fully confined fractures. However, it differs in the way in which the fracture propagates in the 3D space. They assume plane strain in the horizontal direction, which implies that the fracture width changes more slowly in the vertical direction than in does in the horizontal direction. In practice, this is true if the fracture height is much larger than the fracture length. This results in fracture geometry with an elliptical cross section in the horizontal plane and just rectangular in the vertical plane. The fracture height is also assumed to be constant and the same size as the reservoir thickness.

Model	Assumptions	Shape	BH Pressure	Application
PKN	Fixed height Plaine Strain	Elliptical Cross Section	Increasing with time	Length >> Height
KGD	Fixed height Plaine Strain	Rectangular Cross Section	Decreasing with time	Length << Height
Radial	Uniform distribution of Fluid pressure Constant injection rate	Circular Cross Section	Decreasing with time	

Table 1: Comparison between traditional hydraulic fracture models (Ge, 2009).

For the penny-shaped or radial model, the fracture is assumed to propagate in a given plane with the same rate in all directions. The fracture geometry shows a circular cross section and is symmetrical with respect to the point of fluid injection. It is assumed that the distribution of fluid pressure is uniform within the plane and the injection rate should be constant (Abé, 1976).

2.2.3 WELL PERFORMANCE

The most important output parameter within the scope of economic feasibility and technical performance of a geothermal doublet is the generated geothermal power. The geothermal power that is extracted at the surface extractor depends on the drop between the production temperature and the injection temperature, the mass flow rate of production and the heat capacity of the fluid. This relationship is presented in the following equation.

(9) $\quad P_w = Q_m C \Delta T$

In which Q_m is the mass flow out of the system, and can be calculated by the volumetric injection rate (Q) times the density of the fluid. A doublet is a closed system, and thus the production rate is assumed to be equal to the injection rate of fluids (van Wees, 2012). Besides this mass balance, the performance calculations also assume a pressure balance. In order derive a balanced volume flow; a constant pressure is applied at the surface. This pressure must be sufficient to overcome pressure variation. Pressure variations can be a result of 1) pressure losses by fluid flow into the reservoir between the injector and producer well, 2) pressure variations in the vicinity of the producer and injector due to "skin", 3) pressure effects due to gravitational forces and 4) pressure losses due to friction within the well or reservoir.

Pressure losses within the well can be determined by the fluid resistance; the resistance of fluid to flow from the well into the aquifer. The hydraulic resistivity gives the pressure loss as a consequence of fluid flow into an aquifer with homogeneous properties and is for a doublet system defined as (Fetter, 2001):

(10) $\quad \Delta P = P_{bh} - P_{res} = Q \, \dfrac{\mu}{2\pi k h R_{ntg}} \left(\ln\left(\dfrac{L}{r_{well}}\right) + Skin \right)$

In which P_{bh} is the well pressure (Pa), P_{res} is the initial hydrostatic pressure in the reservoir (Pa), μ is the fluid viscosity (Pa s), k is the reservoir permeability (m^2), h is the reservoir thickness or reservoir thickness penetrated by the well (m), R_{ntg} is the net to gross ratio (-), L is the lateral well distance (m), r_{well} is the outer well radius (m), Skin is the skin factor and Q is the volumetric flow rate (m^3/s). The distance between the wells should be chosen as such that a thermal breakthrough is prevented during the lifetime of the doublet. A thermal breakthrough occurs as soon as the cooled front reaches the producer well and cold fluids start to be extracted instead of hot fluids or steam. Generally, the wells are placed well over 1 kilometre in distance.

Properties in the vicinity of the wells are often deviating from those in the rest of the reservoir due to drilling and well completion (van Everdingen, 1953). These effects are combined in the skin factor. The skin factor is a dimensionless value that includes the effect of processes that influence the productivity of a well. A negative skin actually has a positive effect on the well productivity, as it enables enhanced flow rates without enhancing the pump pressure of the system. The pressure change due to skin can be singled out from equation 10.

(11) $\quad \Delta P_{skin} = Q \, \dfrac{\mu}{2\pi k h R_{ntg}} Skin$

Well-clogging or flow barriers may result in an associated pressure drop – a positive skin - which decreases the productivity of a well. Well stimulations aims at mitigating skin related pressure drops, preferably towards removing near well damage and increasing the well performance accordingly

(negative skin). Negative skin can be achieved through sub-horizontal drilling, natural fractures in the system and hydraulic fracturing. In order to show how the skin factor contributes to the geothermal power of the system, we used the DoubletCalc simulators provided by TNO. (Veldkamp J. P., 2015). It is capable of analytically calculating the expected geothermal power of a geothermal doublet system if one knows the site-specific input parameters. We used arbitrary chosen field parameters as input (Appendix B). We varied the input for the skin factor of the injector and compared it to a case with zero skin. **Figure 7**: shows the effects of a positive and negative skin on the potential geothermal power production of a geothermal well system. The results are subdivided into the P90, P50 and P10, which represent respectively a 90%, 50% and 10% probability of that geothermal power production. It shows that a negative skin has a positive influence on the produced geothermal power, whereas a positive skin reduces the geothermal power. The relationship between the skin factor and the geothermal power is non-linear.
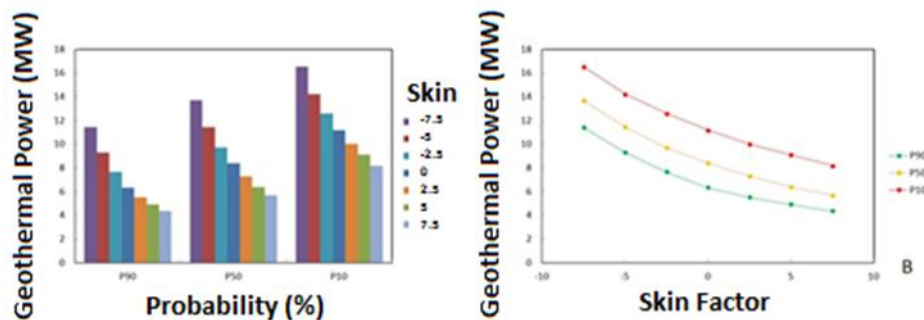

Figure 7: Skin analysis of a hypothetical geothermal field by DoubletCalc. A) Geothermal power production for the P10, P50 and P90 probabilities as a result of skin factor. B) Geothermal power production for each skin factor for all three probabilities; P90, P50 and P10. Field parameters can be found in appendix B.

As can be obtained from the expressions above, the performance of a geothermal project is highly affected by the permeability, temperature and pressure of a reservoir. These parameters are all affected by the depth of the geothermal reservoir. The permeability of rock for instance decreases considerably with depth, and thus has a negative effect on the expected performance (Eq.10). On the other hand, temperature actually increases with depth, and higher temperature differences between the injection and production temperature of the brine fluids increase the generated geothermal power (Eq. 9). This results in a linear increase in performance of a geothermal doublet with depth. For shallow reservoirs, the low temperature difference dominates the reduction in geothermal power, whilst for deep reservoirs; the reduction in performance is dominated by the decrease in porosity and permeability. Studies have shown, that there is a trade-off as such that an optimal depth can be found for which the performance of a geothermal doublet is highest for the temperature and permeability distribution in depth. However, for low permeability reservoirs, the well production can actually be increased by reservoir stimulation or adapted well design (Eq. 11). The potential increase in well productivity as a result of hydrothermal stimulation if further elaborated on in chapter **Fout! Verwijzingsbron niet gevonden.**.

2.3 RISKS AND UNCERTAINTIES

Predictions of stimulation jobs always carry uncertainties and risks; economical, environmental, technical, but also for the local populations. Production of geothermal doublets has an impact on surface movement, due to compaction or extension of the affected formation, and may result in the reactivation of faults and induced seismicity in and around the geothermal reservoir. This raises safety concerns by an increased risk of water flooding and constructional damage - to houses and buildings as well as geothermal wells and operation equipment. Knowledge about the risk and size of subsidence and seismicity is thus essential in geothermal reservoir management. It is therefore

important to get more insight in these mechanisms in order to minimize their impact and mitigate the risk for operations and public safety. An additional model was developed to get an insight in the effects of compaction, subsidence and induced seismicity and is further elaborated in chapter 4.

2.3.1 COMPACTION AND SUBSIDENCE

Reservoir compaction, accompanied by surface subsidence, has long been known as a result of operations around oil and gas reservoirs. For instance, the Goose Creek oil and gas field in Texas has led to dramatic subsidence between 1918 and 1925 as a result of fluid extraction (Pratt, 1926). At another field, the Wilmington field below Long Beach in California, almost 10 meter of subsidence was experienced after lowering the reservoir pressure during exploitation in the early 1960's (Allen, 1968). At this location further subsidence was avoided by the injection of water to maintenance the net pressure in the field.

Large amounts of subsidence have also been observed in areas where geothermal heat was produced without compensating with injection operations (Fokker, 2015). Injection should therefore be performed, amongst others, to maintenance the reservoir pressure and when the production and injection rates are equal, the average pressure in the field will remain the same. However, the fluid pressure will increase locally around the injection well and decrease around the production well. This still has poro-elastic effects, as described in section 2.2.1., and may result in dilation of the reservoir rock. On the contrary, the cooling of the rock around the injection well results in contraction of the reservoir rock. When the pressure distribution is rather stationary, the thermal effects are expected to be the largest contributing factor.

2.3.2 INDUCED SEISMICITY ON PRO-EXISTING FAULTS

Besides forming a risk for surface subsidence, reservoir compaction also increases the potential on induced seismicity in and around the reservoir. Large scale geothermal heat production from subsurface reservoirs may result in considerable fluid pressure and temperature perturbations and concern has been raised over whether nearby faults, that are optimally orientated relatively to in situ stress components, could be reactivated with shear failure (Mode II and III in **Figure 4**). Incidents of fault reactivation due to fluid injection has been known in various sites worldwide, such as Rangely and Denver in Colorado, Geyser geothermal fields in California, Cooper Basin in Australia, Basel in Switzerland and Soultz-Sous-Forêts in France (Baisch, 2006)(Ellsworth, 2013)(Healy, 1968)(Majer, 2007)(Raleigh, 1976)(Cladouhos, 2010). The seismic response can occur almost immediately after the onset of activities or can happen within a time delay ranging from hours to several years. Seismic activity forms a risk when the acceleration at the surface resulting from a seismic event is sufficient to damage infrastructure or population (Majer, 2007). Earthquakes with magnitudes $M_w < 1$ are therefore generally not dangerous, however there are exceptions possible.

Pre-existing faults can be reactivated when the shear stress on the fault exceeds the shear strength of the fault. Each fault plane has a shear stress which acts parallel to the plane and a normal stress which acts perpendicular, or normal, to the fault plane. These can be calculated from the maximum and minimum principal stresses (σ_1 and σ_3) by the following equations:

$$(12) \quad \tau = \frac{\sigma_1 - \sigma_3}{2} \sin(2\theta)$$

With the symbols being
τ = Shear stress on the fault [Pa]
σ_n = Normal stress on the fault [Pa]

$$(13) \quad \sigma_n = \frac{\sigma_1 + \sigma_3}{2} - \frac{\sigma_1 - \sigma_3}{2} \cos(2\theta)$$

θ = Dip of the fault w.r.t. σ_1 direction [°]

Then, the condition of failure and the onset of fault slip is usually expressed as the Mohr-Coulomb failure criterion (Jaeger, 2007). This criterion is approximated as follows:

(14) $\tau_c = \mu_f(\sigma_n - \alpha P_f) + S_o = \mu_f \sigma'_n + S_o$

In which τ_c is the critical shear stress for slip to occur, μ_f is the friction coefficient of the fault and normally lies around 0.6 to 1.0 for most rock, σ_n is the normal stress acting on the fault plane and P_f is the pore pressure fluid. The contribution of fluid pressure to the stress change is defined by the Biot's coefficient α. S is the cohesive strength of the rock [Pa] and is expected to be 0 for pre-existing faults. σ'_n is the effective normal stress, which is simply the normal stress minus the pore fluid pressure. The failure criterion shows that increasing the shear stress, reducing the normal stress, increasing the pore pressure and/or reducing the friction coefficient or cohesion of the fault can bring a fault to failure (TNO, 2014). Various physical mechanisms can lead to fault reactivation and induced seismicity; 1) pore pressure increase, 2) poro-elastic stress changes, 3) thermal stress changes, 4) differential compaction, 5) mass changes, 6) stress transfer from nearby earthquakes and 7) chemical reactions (McGarr, 2002). Depending on the initial local geological conditions and the type of subsurface operations, one of these mechanisms can be dominant of one another or several mechanisms can be operating simultaneously. In this study we will only focus on the first four mechanisms.

Figure 7 shows the effect of cold fluid injection on failure of a pre-existing normal fault with a Mohr-Coulomb representation. This faulting regime is most relevant for the Dutch subsurface, where the vertical stress is larger than the horizontal stresses, as further explained in chapter **Fout! Verwijzingsbron niet gevonden.**. The Mohr circle is defined by the minimum principal stress (left intersection of circle with the x-axis) and the maximum principal stress (right intersection of circle with the x-axis). The area in between the failure line in referred to as the Mohr-Coulomb envelope and is defined by the critical shear stress of the fault. All stress states that fall within this zone do not give rise to failure. As soon as the stress state is as such that the Mohr circle touches the failure line, i.e. the shear stress on the fault exceeds the fault strength, the fault will fail and a seismic event will be generated. If the circle touches the failure line at the right side of the y-axis the fault will fail in shear. As soon as the circle crosses towards the left of the y-axis, i.e. if the minimum effective principal stress is smaller than the pore fluid pressure present, this will lead to tensile failure. This latter is expected for the formation of hydraulic fractures as described in section **Fout! Verwijzingsbron niet gevonden.**. The Mohr-Coulomb criterion assumes that the principal stress σ_2 has no influence on whether the fault will fail or not.
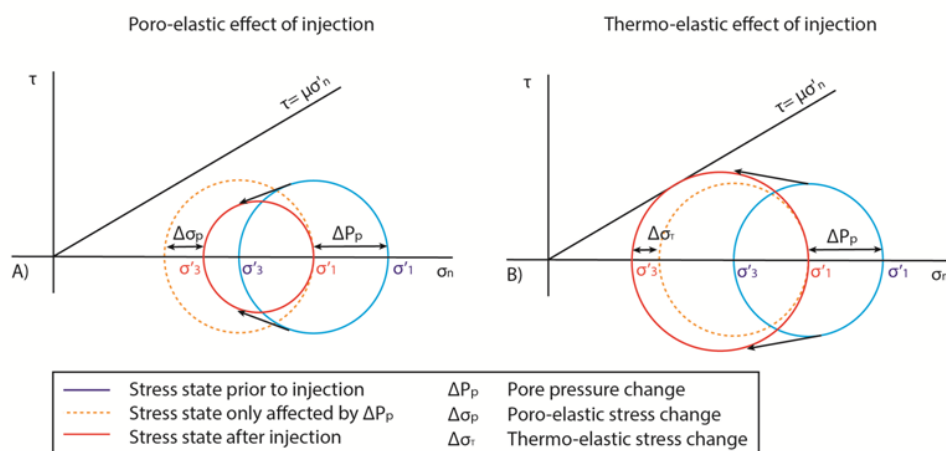
Figure 7: Mohr-coulomb representation of a hypothetical normal fault. Combined with the effect of pore pressure increase A) shows the poro-elastic stress changes and B) the thermo-elastic stress changes during cold fluid injection. Note that the stress changes are chosen arbitrary and do not directly correlate to physical stress changes in nature.

Injection of cold fluids results in a increase of the pore fluids and a decrease of temperature around the well bore. **Figure 7** shows how this affects the stress state on the fault. In the affected area of the reservoir, the pore pressure results in a decrease in both the effective overburden stress and the effective minimum horizontal stress. In the Mohr-Coulomb representation this causes the Mohr circle to shift towards the left, towards the failure line. Simultaneously the change in pore pressure also results in an increase in volume of the reservoir rock, which results in an increase in minimum horizontal stress. It does not affect the overburden stress (TNO, 2014). The magnitude of this stress change corresponds to the defined stress path ratio γ_h as explained in section **Fout! Verwijzingsbron niet gevonden.**. This is only a fraction of the total fluid pressure change, and if the total stress change is not sufficient, this could bring the fault further away from failure. The Mohr circle then shrinks during fluid injection (**Figure 7**A). Cooling of the reservoir rock has the opposite effect. Cooling leads to contraction of the rock formation and a decrease of the horizontal stresses. The size of this stress change depends on the thermal expansion coefficient, the temperature change and the bulk modulus K of the reservoir. In a normal faulting regime, the Mohr circle than grows and the shear stress may converge onto the failure line.

Thermal stresses are relevant in near-well areas and largely contributing in geothermal reservoirs, as the temperature difference is especially large in these operations.

Differential Compaction
Studies have shown that reservoir compaction, as a result of stress changes near the well, also induces stress changes in the surrounding rock formation at locations beyond the thermally affected area (Segall, 1998). Reducing the rock volume in one location, results in extension of neighbouring rock. Otherwise it would leave a void. This contraction also changes the stress conditions in the surrounding rocks and this is most severe around the edges of the affected area. In case of geothermal systems these locations are at the upper and lower boundaries of the reservoir and at the edges of the thermal front or at fault boundaries (**Fout! Verwijzingsbron niet gevonden.**).

In the past many analytical and numerical geomechanical studies have been executed on the stress effects in and outside the reservoir, relate to specific reservoir geometries. From analytical approaches it has become clear that the effective stress changes due to differential compaction are not in agreement with the stress changes with uniaxial assumptions as proposed in the previous section.

This is especially the case for areas close to the edges of the reservoir. Since the vertical and horizontal stress change at different rates during injection or depletion of a reservoir, stress arching occurs at these locations. This means that a part of the overburden load, which was previously carried by the reservoir itself, is transmitted to the side during reservoir compaction (Soltanzadeh, 2008). In reservoir depletion and accompanied compaction, the edges of the reservoir compartments (*Figure 9*), show stress changes up to one magnitude higher that central-reservoir changes (Orlic, 2011; Orlic, 2009). In the case of injection, poro-elasticity results in the exact opposite effect, but thermal effects are expected to produce similar results as fluid extraction. Studies by (Soltanzadeh, 2008) (Mulders, 2003) (Mulders, 2003) and (Orlic B. W., 2013) have shown that differential compaction and accompanied stress arching can result in induced seismicity if the reservoir is bounded by a fault.
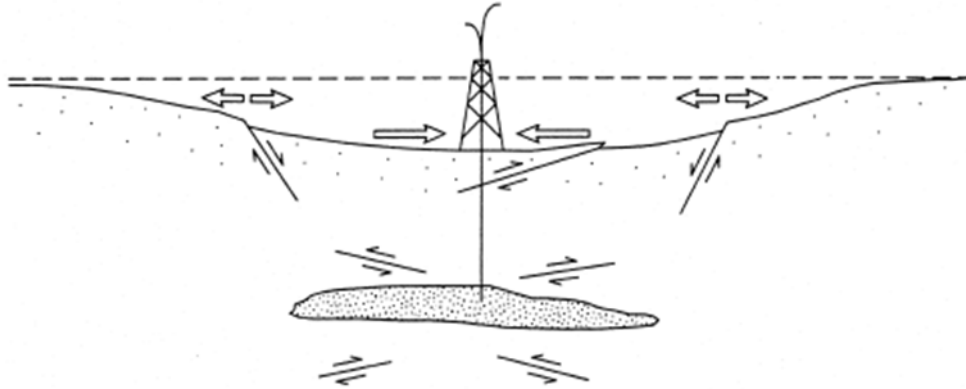

Figure 8 : *Observed faulting associated with fluid withdrawal. This is promoted by reservoir compaction. Normal faults develop on the flanks of the reservoir if the field is located in an extensional environment, whereas reverse faults develop above and below the reservoir in compressional environments (Segall, 1998).*

Soltanzadeh and Hawkes (2008) presented a semi-analytical analysis for reservoirs with rectangular and elliptical cross-section geometry in the x- and y- direction with plane strain conditions in the z-directions, which can be used to define the stress changes inside and outside the reservoir with respect to the pore pressure change. The effective stress change tensor $\Delta\sigma'_{ij}$ is related to the pore pressure change ΔP and the total stress change $\Delta\sigma_{ij}$ as follows:

(15) $\quad \Delta\sigma_{ij} = \Delta\sigma'_{ij} + \alpha\Delta P\delta_{ij}$

In which α is the Biot's coefficient, the subscript ij defines the direction of the stress. For which if ij = 11, the stress in the direction of the maximum principal stress is assumed and ij = 33 assumes the stress in the direction of the minimum principal stress. δ_{ij} is the Knonecker delta, which is taken to be 1 is case of i = j and 0 is i ≠ j.

If the reservoir is a free body, effective stress changes would simply result in contraction or expansion. However, when the reservoir is attached to the surrounding rock, by for instance a sealing fault, no pore pressure changes occur outside the reservoir. The ratio of the total stress change to the change in pore pressure within the reservoir is referred to as the stress arching ratio (Mulders, 2003). These parameters were given a more general form in the paper of Soltanzadeh and Hawkes (2008), who define the normalized stress arching ratios as:

(16) $\quad \gamma_{a(ij)} = \dfrac{\Delta\sigma_{ij}}{\alpha\Delta P}$
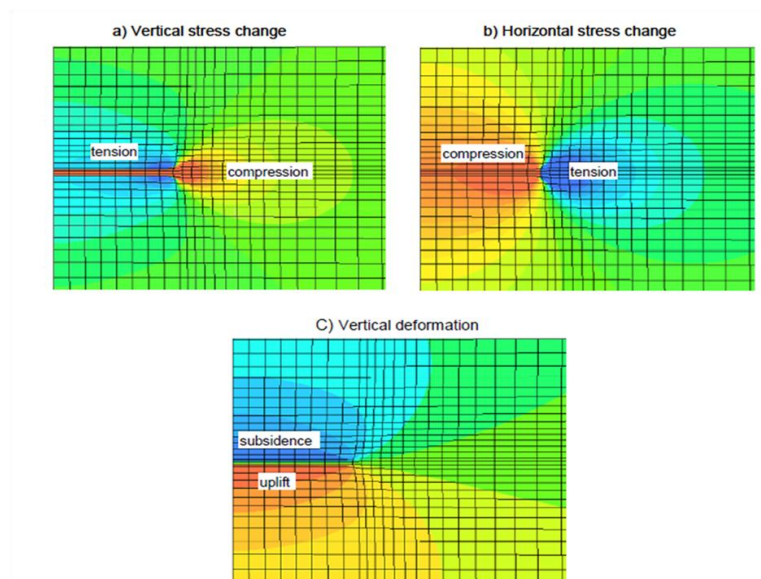
Figure 9: A) Vertical stress change and B) horizontal stress change due to reservoir depletion. Compressive stresses are taken to be negative. Injection into a reservoir results in the opposite effects. C) Vertical deformation due to reservoir depletion in the form of reservoir compaction and subsidence above the reservoir, and uplift below the reservoir. (Orlic, 2011)

Assuming that the normalized stress arching ratios are defined, equation 12 and 13 can be rewritten for the effective stress changes within the reservoir where pore pressure changes are present and stress changes outside the reservoir where pore pressure changes are assumed to be 0.

(17) $\Delta\sigma'_{ij} = \alpha\big(\gamma_{a(ij)} - \delta_{ij}\big)\Delta P$ Inside the reservoir

(18) $\Delta\sigma'_{ij} = \alpha\gamma_{a(ij)}\Delta P$ Outside the reservoir

3 HYDROTHERMAL STIMULATION TOOL

Geothermal energy production can be enhanced by the stimulation of the reservoir. This can be done by hydrothermal fracking (section 2.2). This technique uses the pressure and temperature changes around the wellbore to induce sufficient stress changes to initiate vertical fracture growth within the reservoir. This enhances the permeability of the reservoir and increases the productivity of the injection well, which may have a large economic impact on the geothermal project.

We developed a semi-analytical, predictive tool for first order approximations of the fracture length, skin of the well and the well productivity within a single layer homogeneous and isotropic reservoir. The tool can be used by operators prior to geothermal reservoir production. Knowing the potential gains for production and injection of such a treatment prior to site development is very useful for selecting the optimal site and treatment schedule. For instance, using different injection temperatures, injection rates and pressure, or duration of stimulation may successfully increase the potential of a geothermal operation. And thereby it could also be used to define the best balance between price and quality, since thermal stimulation is relatively cheap.
The theory behind- and the development of the tool are described in this chapter.

3.1 MODEL SET-UP

The pressure and temperature changes within the reservoir, due to fluid- and heat flow, change the stress conditions in the subsurface. The distribution of temperature and pressure are approximated by the Lauwerier's solution and Theis function as described by (Koning, 1988). The stress changes as a result of pressure and temperature changes are calculated based on the plane strain assumption in the approximation of (Perkins T. G., 1985). Fracture initiation and propagation is then derived from the PKN approximation, with one application that includes leak-off along the fracture to determine the length and one approximation that numerically solves the fracture length for the stresses at the fracture tip. The last application is more realistic for high temperature and stiff reservoirs, which is very appropriate for (enhanced) geothermal reservoirs. The tool provides insight in the development of hydrothermal fractures and their effect on the skin of the well and the increase in well productivity due to stimulation.
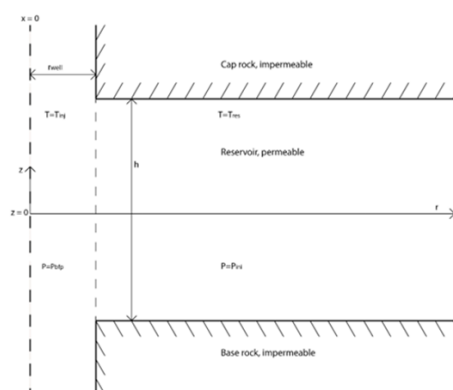

Figure 10 : *Geometry of model. A horizontal, infinitely extending, permeable reservoir rock is bound at the top and bottom by an impermeable cap and base rock. The reservoir has a height h and an initial P&T. The well is located at x=0.*

3.2 GENERAL ASSUMPTIONS

In order to model hydrothermal fracturing of a geothermal field one has to make some simplifications with respect to a real case in nature. Therefore some important assumptions were made, which are listed below:

- Prior to injection the reservoir conditions are at steady state
- The reservoir is an infinite radial symmetric disc with a fixed height h. The reservoir is confined at the top and bottom by an impermeable rock layer – i.e. the cap and base rock.
- The reservoir is a single layer and is linearly elastic, isotropic, homogeneous and permeable and fully penetrated by a vertical well.
- The initiated fracture is assumed to be vertical with a fixed height, which is equal to the height of the reservoir. Thus, leading to no variation in flow in the vertical direction, making this a 2D model. The well is located at the axis of the fracture
- The fracture is approximately planar (i.e. storage in the fracture can be neglected), and its horizontal extent is finite.
- Water from the aquifer flows out of the fracture at the same rate per unit area (a uniform flux exists along the fracture, or the fracture conductivity is high although not infinite)
- The reservoir is linear elastic. Therefore poro-elastic and thermo-elastic stress perturbations can simply be added to the linear elastic stress equations and as extra component.
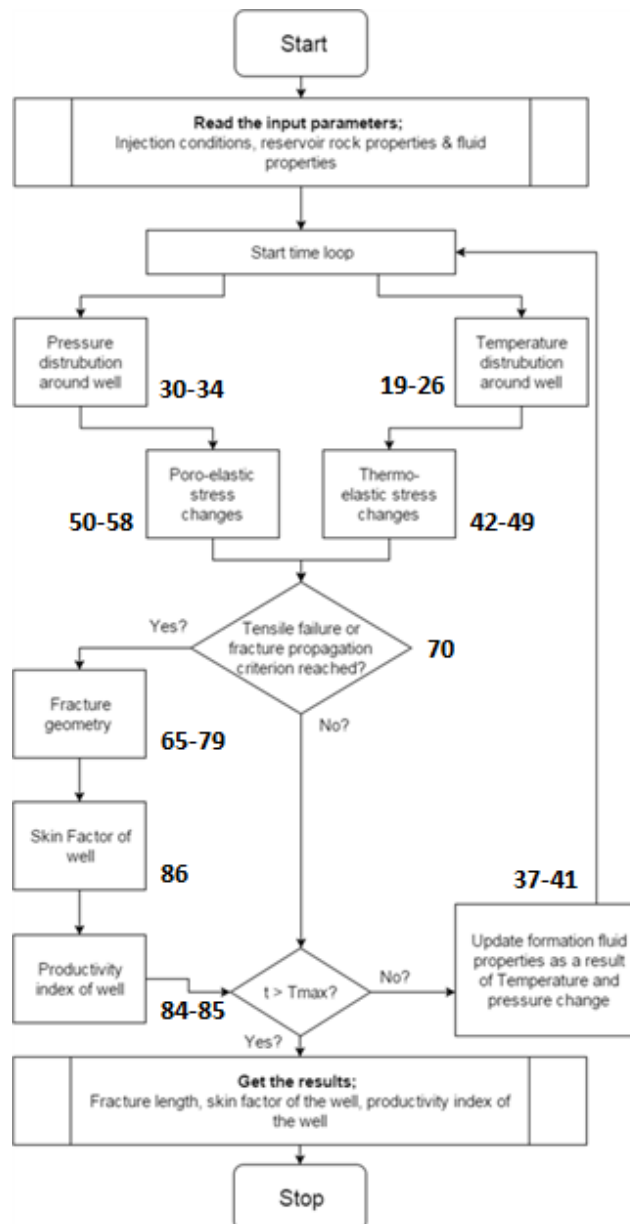
Figure 11: Flow chart of the tool. Note that all numbers correspond to the equations that are solved during this step. The equations can be found in this chapter.

3.3 GOVERNING EQUATIONS

The following aspects and mechanisms are included in this tool. The mechanisms are solved in the order shown below, as can also be seen in the flow chart of **Figure12**. The equations used are described in detail in this section:

- Distribution of the temperature and pressure front around the well bore due to cold fluid injection.
- Behaviour of formation fluids as a result of temperature, pressure and salinity at each location in time.
- Induced stress changes accommodated by pressure and temperature changes.
- Fault opening by the tensile failure criterion as a result of changing stresses and pressure at the wellbore.

- Fracture propagation in time, which is a complex mechanism that depends on the fluid and heat flow within the fracture and simultaneous fluid leak of into the rock formation.
- Well productivity increase as a result of fracture growth.

3.3.1 TEMPERATURE DISTRIBUTION AROUND THE WELL BORE

The temperature field around the well bore is determined by Lauwerier's solution in radial (or cylindrical) coordinates (Koning, 1988). This applies to injection of an incompressible fluid, such as water, at a constant injection rate. One-dimensional vertical heat conduction from the overlying cap- and underlying base rock is taken into account, whilst horizontal heat conduction can be neglected. The temperature is assumed to be constant over the whole reservoir thickness, i.e. in the vertical direction, and the bottom hole temperature is taken to be equal to the temperature of the injective (Van den Broek, 2015). Thus, there is no heat loss or gain inside the well.

$$(19) \quad T_D = erfc\left\{\sqrt{\tau_D}\frac{R_D^2}{2(1-R_D^2)}\right\} \qquad R_D < 1; |z| \leq \frac{h}{2} \quad \text{Inside reservoir and T front}$$

$$T_D = erfc\left\{\frac{R_D^2\tau_D + z_D}{2\sqrt{\tau_D(1-R_D^2)}}\right\} \qquad R_D < 1; |z| > \frac{h}{2} \quad \text{Outside reservoir/inside T front}$$

$$T_D = 0 \qquad R_D \geq 1; -\infty < z < \infty \qquad \text{Outside the T front}$$

$$(21) \quad \Delta T = 0 \qquad T_D > 1$$

$$\Delta T = (T_{inj} - T_{res})T_D \quad T_D > 1$$

$$(22) \quad T = T_{res} + \Delta T$$

$$(23) \quad R_D = \frac{r}{R_c}$$

$$(24) \quad \tau_D = \frac{4\alpha_{cap}tC_{cap}^2}{h^2 C_{res}^2}$$

$$(25) \quad R_c = \left(\frac{C_{inj}}{C_{res}}\frac{Qt}{h\pi}\right)^{\frac{1}{2}}$$

$$(26) \quad \Delta z_D = \frac{C_{res}}{C_{cap}}\left(\frac{2z}{h} - 1\right)$$

With the symbols being:

T_{res} = Reservoir temperature [°C]
T_{inj} = Injection temperature [°C]
ΔT = Temperature change as result of injection [°C]
T_D = Dimensionless temperature coefficient [-]
R_D = Dimensionless radius coefficient [-]
r = Distance from well [m]
R_c = Radius of temperature front [m]
τ_D = Dimensionless coefficient [-]
α_{cap} = Thermal diffusivity of cap and base rock [m²/s]
t = Injection time [s]
h = Reservoir height [m]
C_{res} = Heat capacity of filled reservoir rock [J/m³ °C]
C_{cap} = Heat capacity of cap and base rock [J/m³ °C]
C_{inj} = Heat capacity of injection fluid [J/m³ °C]
Q = Injection rate [m³/s]
z = Reservoir depth [m]
Δz_D = Dimensionless coefficient of depth [-]

R_c is the radius of the temperature front and is derived from a simple heat balance equation (Eq. 27), in which the heat absorbed by the injection fluid is equal to the heat given off by the reservoir (Koning, 1988). When the distance from the wellbore (r) approximates R_c, the total temperature difference goes to zero.

$$(27) \quad QtC_{inj}\Delta T = \pi R_c^2 h C_{res}\Delta T$$

According to (Koning, 1988) the horizontal heat conduction can be neglected if the radial velocity of the temperature front is much greater than the vertical velocity of the temperature transient in the over and underlying rocks. With isotropic thermal conductivities and approximately equal thermal diffusivities of the reservoir, cap and base rock, horizontal heat conduction can be neglected. This condition is met if the Peclet number (Pe) is larger than 1 (Eq. 28). Inserting the expression for R_c in this equation than gives equation 29, which is met for most field conditions.

$$(28) \quad Pe = \frac{C_{res}R_c^2}{C_{cap}\alpha_{cap}t} \gg 1 \qquad\qquad (29) \quad \frac{C_{inj}Q}{C_{cap}\alpha_{cap}h\pi} \gg 1$$

The dimensional time parameters T_D is plotted against the dimensionless radius R_D for different values of τ_D in figure XX. The plot shows that for small values of τ_D, smaller than 0.05, the step function is a accurate approximation of the temperature profile within the reservoir. In other words, the temperature profile shows the maximum distance from the well for which heat transfer through convection is applicable. Within this temperature front the amount of heat given off by cap and base rock is small with respect to the amount of heat given off by the reservoir (Koning, 1988).
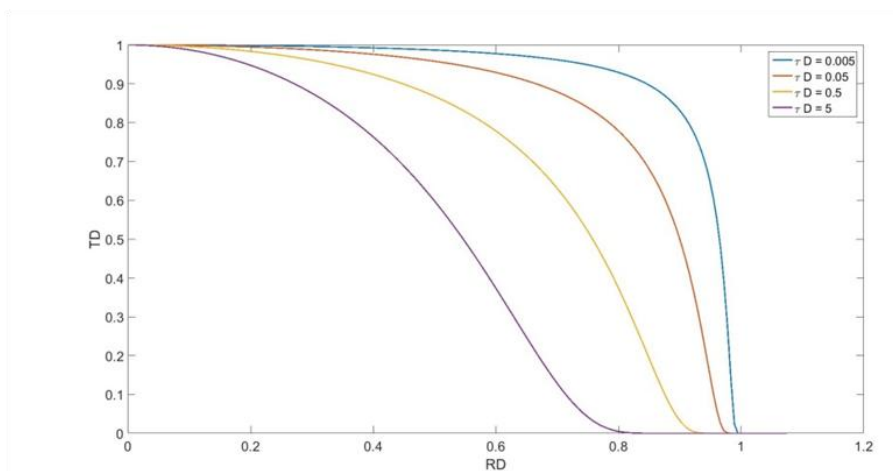

Figure 12: *Lauwerier's temperature profiles within the reservoir for various values of τ_D. Plotted against the dimensionless radius R_D.*

3.3.2 PRESSURE DISTRIBUTION AROUND THE WELL

During the pumping or injection of water into a subsurface aquifer, the hydraulic head in the observed in the well will change. This is referred to as the drawdown of the well. The first mathematical analysis of transient drawdown effects in a confined aquifer was published by (Theis, 1935). The function solves the non-stationary flow within a reservoir and we use the same function to determine the pressure distribution around the well bore. It follows some simple assumptions (Fetter, 2001):

- The geologic aquifer is horizontal and has an infinite extent. Thereby the aquifer is bounded at the top and the bottom by a confining layer.
- The aquifer is homogeneous and isotropic and fluid flow is solved radially towards or from the well.
- Darcy's law for fluid flow is valid
- The aquifer is compressible and water is directly released into the aquifer as the head is increased due to injection. The opposite is true for production.

Theis' function is further defined by (Kruseman, 1994), who shows that the rate of increase of hydraulic head, multiplied by the storativity – the product of the specific storage and the aquifer

thickness – and summed of the area of influence, equals the fluid recharge into the formation. This is written in an exponential integral (Eq. 33).

(30) $S = \rho_{inj} g h (c_t + \varphi c_{inj})$

(31) $T_r = \dfrac{k \rho_{inj} g}{\mu}$

(32) $u = \dfrac{r^2 S}{4 T_r t}$

(33) $s = \dfrac{Q}{4 \pi T_r} \displaystyle\int_u^\infty \dfrac{e^{-y}}{y} dy$

(34) $\Delta P = \rho_{inj} g s$

(35) $P = P_{init} + \Delta P$

With the symbols being:

S $\quad$ = Storativity
ρ_{inj} $\quad$ = Density of injection fluid [kg/m^3]
g $\quad$ = Gravitational acceleration [m/s^2]
ϕ $\quad$ = Porosity [-]
c_{inj} $\quad$ = Compressibility of injection fluid [Pa^{-1}]
c_t $\quad$ = Total reservoir compressibility [Pa^{-1}]
T_r $\quad$ = Transmissivity [m^2/d]
k $\quad$ = Permeability [D]
μ $\quad$ = Viscosity [Pa·s]
Q $\quad$ = Injection rate [m^3/d]
s $\quad$ = Well drawdown [m]
ΔP $\quad$ = Pressure change as result of injection [Pa]
P_{init} $\quad$ = Initial reservoir pressure [Pa]

The Theis function is solved by executing equations 30 to 34 in space and time. These equations define the specific storage (30), the transmissivity (31) and argument u (32). The latter is necessary to solve the exponential integral by using the analytical equations below. In these equations λ is the Euler-Macharoni constant and is taken to be 0.5772156649.

$$\int_u^\infty \frac{e^{-y}}{y} dy = \ln\left(\frac{e^{-\lambda}}{u}\right) + 0.9653u - 0.1690u^2 \qquad u \leq 1$$

$$\int_u^\infty \frac{e^{-y}}{y} dy = \frac{1}{ue^u} \frac{u + 0.3575}{u + 1.2800} \qquad u > 1$$

Once the drawdown s in the well is defined, this can be converted to the pressure change by equation 34. In the end this is added to the initial pore pressure of the reservoir to get the total pore pressure distribution within the reservoir through time.

3.3.3 CHARACTERISTICS OF FORMATION FLUIDS

Theis' function and the Lauwerier's solution both use constant fluid characteristics in time. Though, as already mentioned in section **Fout! Verwijzingsbron niet gevonden.**, chemical effects as a result of changing temperature, pore pressure and salinity of the subsurface fluids do affect the fluid chemistry and behaviour and play therefore an important role in geothermal reservoirs. From literature, (Adams, 2002) (Batzle, 1992) (Sun, 2008), we found suiting expressions to determine the effects of P, T and salinity of the reservoir on the density, viscosity and heat capacity of the formation fluids. These empirically derived functions are incorporated in the tool.

Salinity of formation water
The salinity of the formation water is initially static and can be expressed as a function of the depth and thickness of the aquifer. With the following expression one can approximate the salinity of the initial reservoir fluid, in which h is the aquifer thickness, Z_{res} is the depth and Z_{top} is the depth till the top of the aquifer. For the middle of the reservoir $Z_{res} = Z_{top} + 0.5h$.

$$(36) \quad TDS(Z_{res}) = TDS_{aq} \frac{Z_{res}}{Z_{top} + 0.5h}$$

Density of formation water

The most fitting approximation of the density changes due to pressure, temperature and salinity is provided by (Batzle, 1992) and (Adams, 2002). For a large range of P, T and TDS, they gave the following expression for the density of freshwater at different T&P (ρ_w) and freshwater with different T&P&TDS (ρ_b). ρ_w and ρ_b are in g/cm^3, S is NaCl mass fraction (ppm/1e^6), P is in MPa and T is in °C.

$$(37) \quad \rho_w = 1 + 1e^{-6}(-80T - 3.3T^2 + 0.00175T^3 + 489P - 2TP + 0.016T^2P - 1.3e^{-5}T^3P - 0.333P^2 - 0.002TP^2)$$

$$(38) \quad \rho_b = \rho_w + S(0.668 + 0.44S + 1e^{-6}(300P - 2400PS + T(80 + 3T - 3300S - 13P + 47PS)))$$

Viscosity of formation water

(Batzle, 1992) also developed an expression for the viscosity of solutions. They considered the pressure effect to be negligible small and therefore did not incorporate this in the equation. Viscosity at different T&TDS is then defined as

$$(39) \quad A = (0.42(S^{0.8} - 0.17)^2 + 0.045)T^{0.8}$$

$$(40) \quad \mu_b = 0.1 + 0.333(S + (1.65 + 91.9)S^3)e^{-A}$$

in which μ_b is in cP, S is the NaCl mass fraction (ppm/1e6) and T is in °C.

Heat conductivity of formation water

The heat capacity of brine is also dependent on the temperature, salinity and pressure. (Grunberg, 1970) developed and expression to establish the heat capacity of brine water and (Feistel, 2007) refers to this equation as reliable. C_w is the heat capacity [kJ/kg*K], S is the salinity [g/kg] and T is the temperature in Kelvin.

$$(41) \quad C_w = (5.328 - 9.760e^{-2}S + 4.04e^{-4}S^2) + (-6.913e^{-3} + 7.351e^{-4}S - 3.150e^{-6}S^2)T + (-9.6e^{-6} - 1.927e^{-6}S + 8.230e^{-9}S^2)T^2 + (2.5e^{-9} - 1.666e^{-9}S + 7.125e^{-12}S^2)T^3$$
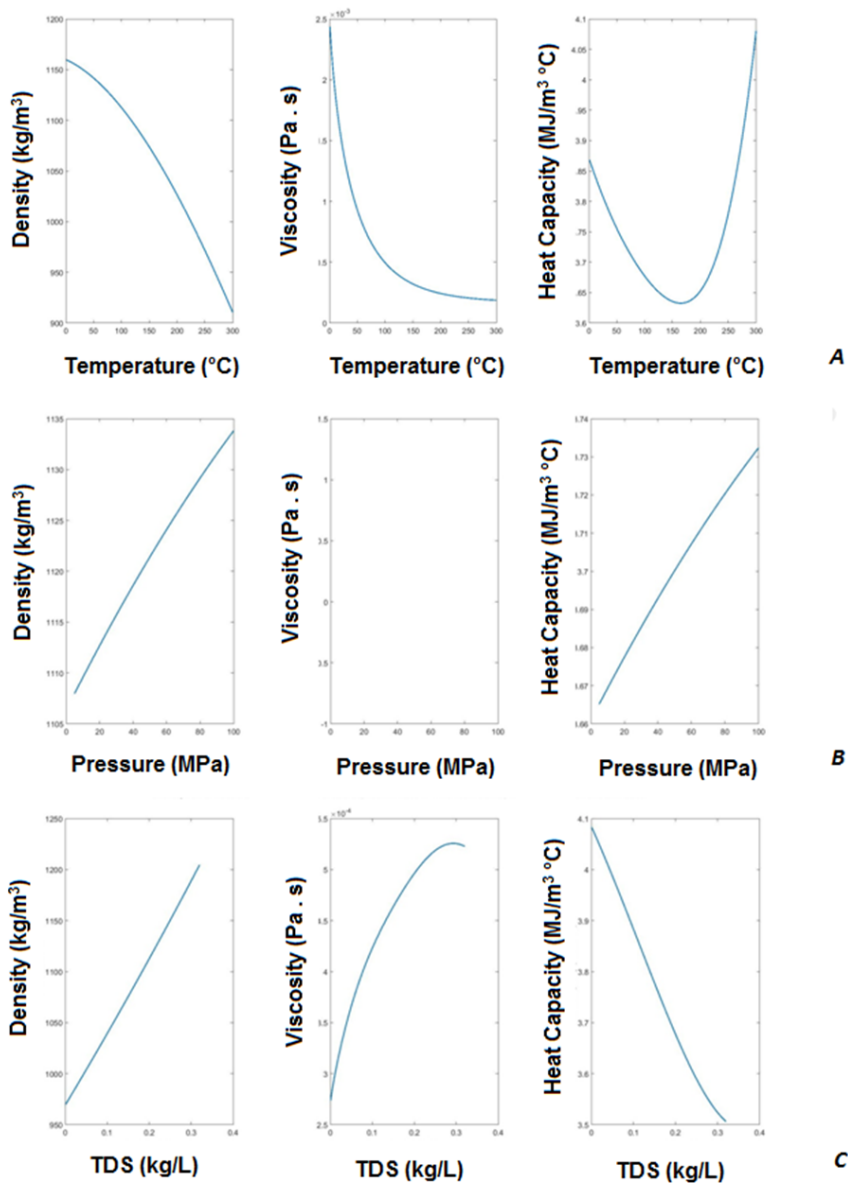
Figure 13: *Effect of temperature (A), pressure (B) and salinity (C) of formation fluids on their density, viscosity and heat capacity. Note that in each case only one parameter is take over a wide range while the other two stay constant. The constants are 100 °C for the temperature, 19.62 MPa for the pressure and 200.000 mg/L for the salinity. The values are calculated after Batzle and Wang (1992) and Feistel (2007). Note that these relationships are not comprehensive for each site as they depend on the input for T, P and TDS, but give a general approximation of the fluid behaviour.*

Figure 13 shows the relations between temperature, pressure and salinity and density, viscosity and heat capacity of the brine fluid according to the equations mentioned above. It displays that an increasing temperature results in a decrease in density and viscosity of the fluid, thereby it also reduces the heat capacity until a critical turning point after which it starts to increase again. Pressure only affects the heat capacity and density of the brine as such that they decrease with increasing pressure. The salinity of the fluid also plays a key role. Increasing the TDS results in a linear increase in density and a semi-linear decrease in heat capacity. The viscosity increases with increasing TDS until it reaches a maximum – turning point – after which it decreases again. Since the TDS is a result

of the depth of burial we generally assume this value to be constant throughout the reservoir, whilst pressure and temperature change in laterally and in time.
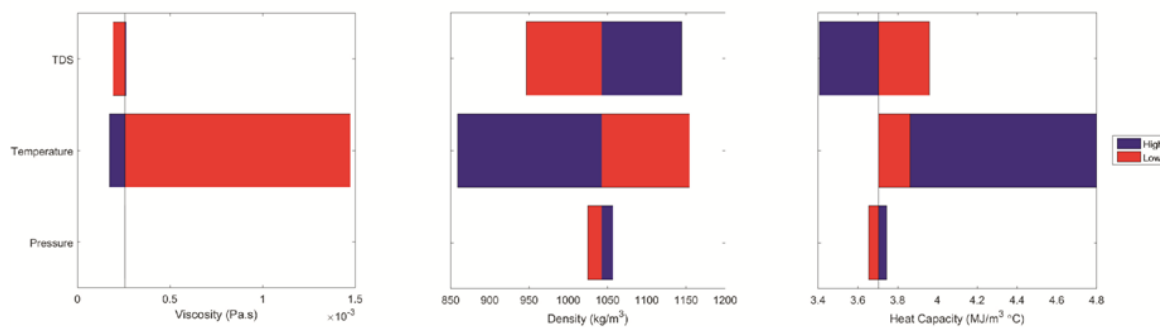

Figure 14: Tornado plot for the viscosity, density and heat capacity as a consequence of temperature, pressure and TDS.

In **Figure 14** a tornado plot shows the viscosity, density and heat capacity against the temperature, pressure and salinity of the fluid. A maximum, minimum are plotted with respect to a base case for each parameter. The base case has a temperature of 185 °C, a pressure of 52.5 MPa and a TDS of 185.000 mg/L. The same ranges are used as in **Figure 14**. Thus, the minimum and maximum for temperature are 20 °C and 350 °C, for pressure they are 5 MPa and 100 MPa and for TDS they are 50.000 mg/L and 320.000 mg/L. The figure shows that viscosity is highly affected by temperature. For low temperatures the viscosity increases significantly. The density is also most affected by the temperature and then the salinity. Low temperatures and high TDS result in low densities. The heat capacity reduces with high salinity and increases with both high and low temperatures. At last, all fluid characteristics are barely or not at all affected by the pressure.

3.3.4 INDUCED STRESS CHANGES IN THE SUBSURFACE RESERVOIR
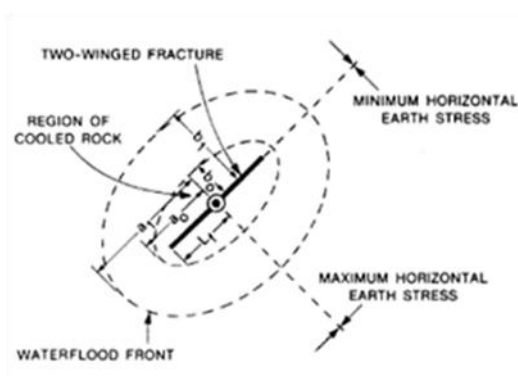
In typical geothermal systems fluids are injected that are relatively colder than the formation temperature. This results in the formation of a cooled front around the well, which grows as additional fluid is injected. As explained in section **Fout! Verwijzingsbron niet gevonden.** cooling leads to contraction of the rock around the well and a reduction of minimum horizontal stress, whilst pore pressure increase results in expansion of the rock volume around the well and increases the minimum horizontal stresses.

Figure 15: Schematic top view of cooled and flooded front in the vicinity of a well during injection. The distribution of the temperature and pressure front grows elliptically as a result of a two-winged fracture. Geometric variables used in calculations are shown in relation to the well bore. From (Perkins, 1985).

(Perkins, 1985) developed expressions for the thermo-elastic stress changes and redefined the stress changes as a result of pressure change. Initially the distribution of temperature and pressure is radially outward from the well, however if injection conditions are as such that a hydraulic fracture is created, then the flow system will evolve from an essentially circular geometry in the plan view to one characterized more nearly as elliptical (*Figure 15*). The semi-axes of the cooled region are determined using the procedure from (Perkins, 1985) by using equations 42 - 45.

The procedure requires the input of a fracture half length, the length of one wing of the fracture. For

$$(42) \quad V_c = \frac{C_{inj}}{C_{res}} qt$$

$$(43) \quad F_1 = \frac{2V_c}{\pi L_f^2 h} + \frac{1}{2}\sqrt{\left(\frac{4V_c}{\pi L_f^2 h}\right)^2 + 4}$$

$$(44) \quad a_c = L_f \frac{F_1^{\frac{1}{2}} + F_1^{-\frac{1}{2}}}{2}$$

$$(45) \quad b_c = L_f \frac{F_1^{\frac{1}{2}} - F_1^{-\frac{1}{2}}}{2}$$

With the symbols being:

V_c	= Volume of cooled region [m^3]
L_f	= Fracture half-length [m]
a_c	= Major axis of cooled region [m]
b_c	= Minor axis of cooled region [m]
e_c	= b_c/a_c Ratio of semi-axis [-]
Co_{H1}	= Factor in stress equation parallel to $S_{h,min}$ [-]
Co_{H2}	= Factor in stress equation perpendicular to $S_{h,min}$[-]
E	= Young's modulus [Pa]
β	= thermal expansion coefficient [°C^{-1}]
ΔT	= Temperature change (T– T_{init}) [°C]
v	= Poisson's ratio [-]
$\Delta\sigma_{bT}$	= Thermo-elastic stress change ⊥ to $S_{h,min}$ [Pa]
$\Delta\sigma_{aT}$	= Thermo-elastic stress change ∥ to $S_{h,min}$ [Pa]

radial flow, in other words before tensile failure, this fracture half-length can be set to the well radius. The well radius is the small distance between the bore hole wall and the center of the well, which is also the cross-section of the two semi-axes. Previous work by (Van den Broek, 2015) has shown that such a small fracture half-length has little to no influence on the shape of the ellipse and the results show a radial symmetric cooled region.

The thermo-elastic stress changes are then numerically approximated according to equation 7, and result is changes in the horizontal directions defined by XX and XX. Since fracture open in the direction of the minimum horizontal stress, it is assumed that the semi-axis define the directions of the minimum horizontal stress and the maximum horizontal stress, as such that a_c is the semi-axis in the S_H direction and b_c in the S_h direction.

$$(46) \quad \Delta\sigma_{bT} = \frac{E\beta\Delta T}{1-v} Co_{H1}$$

$$(47) \quad \Delta\sigma_{aT} = \frac{E\beta\Delta T}{1-v} Co_{H2}$$

$$(48) \quad Co_{H1} = \frac{e_c}{1 + e_c} + \left(\frac{1}{1 + e_c}\right) * \left(\frac{1}{1 + \frac{1}{2}\left(1.45\left(\frac{h}{2b_c}\right)^{0.9} + 0.35\left(\frac{h}{2b_c}\right)^2\right)\left(1 + e_c^{0.774}\right)}\right)$$

$$(49) \quad Co_{H2} = \frac{1}{1 + e_c} + \left(\frac{e_c}{1 + e_c}\right) * \left(\frac{1}{1 + \frac{1}{2}\left(1.45\left(\frac{h}{2b_c}\right)^{0.9} + 0.35\left(\frac{h}{2b_c}\right)^2\right)\left(1 + (1 - e_c)^{1.36}\right)}\right)$$

(Perkins, 1985) empirically derived two factors to give a convenient, explicit method to estimate the average interior stresses in the elliptical cooled regions of any height (Eq. 48 and 49). The factor depends on the ratio of semi-axis e_c and the reservoir height. In case of radial flow these factors for the stress changes are similar in both horizontal principals stress directions. However, they assume that the size of stress changes in both directions differ as soon as a fracture starts growing.

The poro-elastic stress changes are calculated in a similar method as the thermal stresses, provided that the porosity and permeability is assumed to be independent of the stress state (Lubinski, 1954). The relationship between stress change and pore pressure is then define with the linear coefficient of pore pressure expansion, defined as equation 50. This coefficient is analogous to the linear coefficient of thermal expansion β.

$$(50) \quad J = \frac{1 - 2v}{E} - \frac{c_{gr}}{3}$$

In which E is the Young's modulus [Pa] and, v is the Poisson's ratio [-] and c_{gr} is the compressibility of the mineral grains in the reservoir. This right part of the definition is often let out of the equation for simplicity (Van Wees, 2014). Then, the elliptical semi-axes can be solved with the volume of the flooded region, the region that is affected by pore pressure changes.

$$(51) \quad V_{fl} = \frac{qt}{\varphi}$$

With the symbols being:

V_{fl} = Volume of the flooded region [m³]

a_{fl} = Major axis of flooded region [m]

b_{fl} = Minor axis of flooded region [m]

$$(52) \quad F_2 = \frac{2V_{fl}}{\pi L_f{}^2 h} + \frac{1}{2}\sqrt{\left(\frac{4V_{fl}}{\pi L_f^2 h}\right)^2 + 4}$$

J = pore pressure expansion coefficient [Pa⁻¹]

ΔP = Pressure change (P-P$_{init}$) [Pa]

$\Delta\sigma_{bP}$ = Poro-elastic stress change $\perp$ to S$_{h,min}$ [Pa]

$$(53) \quad a_{fl} = L_f \frac{F_2^{\frac{1}{2}} + F_2^{-\frac{1}{2}}}{2}$$

$\Delta\sigma_{aP}$ = Poro-elastic stress change $\parallel$ to S$_{h,min}$ [Pa]

$$(54) \quad b_{fl} = L_f \frac{F_2^{\frac{1}{2}} - F_2^{-\frac{1}{2}}}{2}$$

The poro-elastic can then be calculated according to equation 5. These equations also use a coefficient that relates the ratio of the semi-axes of the flooded area and the reservoir height (Eq. 57 & 58).

$$(55) \quad \Delta\sigma_{bP} = \frac{EJ\Delta P}{1-v}Flo_{H1} = \frac{(1-2v)\Delta P}{(1-v)}Flo_{H1}$$

$$(56) \quad \Delta\sigma_{aP} = \frac{EJ\Delta P}{1-v}Flo_{H2} = \frac{(1-2v)\Delta P}{(1-v)}Flo_{H2}$$

$$(57) \quad Flo_{H1} = \frac{e_{fl}}{1+e_{fl}} + \left(\frac{1}{1+e_{fl}}\right)$$
$$* \left(\frac{1}{1+\frac{1}{2}\left(1.45\left(\frac{h}{2b_{fl}}\right)^{0.9} + 0.35\left(\frac{h}{2b_{fl}}\right)^{2}\right)\left(1+e_{fl}^{0.774}\right)}\right)$$

$$(58) \quad Flo_{H2} = \frac{1}{1+e_{fl}} + \left(\frac{e_{fl}}{1+e_{fl}}\right)$$
$$* \left(\frac{1}{1+\frac{1}{2}\left(1.45\left(\frac{h}{2b_{fl}}\right)^{0.9} + 0.35\left(\frac{h}{2b_{fl}}\right)^{2}\right)\left(1+(1-e_{fl})^{1.36}\right)}\right)$$

3.3.5 TENSION FAILURE CRITERION

As explained in section **Fout! Verwijzingsbron niet gevonden.**, hydrothermal fractures are generated if the pressure in the borehole exceeds the minimum principal stress. In case of a normal faulting, or strike-slip regime, this minimum principal stress will be horizontal and the resulting fracture that is formed will be vertical. During injection, the temperature of the rock around the wellbore decreases, while the pore pressure in this area increases. This affects the strength of the rock and induces stress changes (section **Fout! Verwijzingsbron niet gevonden.**). How these stress changes affect the minimum horizontal stress is described in the previous section.

The borehole pressure, on the other hand, also plays an important role. According to literature, (Ge, 2009) (Koning, 1988) (Veldkamp, 2015) and (Perkins, 1985), the pressure in the borehole, can be calculated with the equations below. These take into account the pressure rises between the borehole and the fracture wall, between the fracture wall and the cooled front and between the cooled front and the flooded front (*Figure 16*). Therefore, they use the semi-axes of the front as calculated in equations 44 and 45.

$$(59) \quad \Delta P_1 = \frac{Q\mu_{hot}}{2\pi kh}\ln\left(\frac{Re}{a_c + b_c}\right)$$

$$(60) \quad \Delta P_2 = \frac{Q\mu_{cold}}{2\pi kh}\ln\left(\frac{a_c + b_c}{L_f}\right)$$

With the symbols being

ΔP_1 = Pressure rise between the cooled and flooded
ΔP_2 front [Pa]
ΔP_{face} = Pressure rise between the fracture wall and
μ_{hot} cooled front [Pa]
μ_{cold} = Pressure rise between the borehole and

$$(61) \quad \Delta P_{face} = 0.00074 \left[\frac{Q \mu_{cold} L_f (E)^3}{(1-v^2)^3 h^4} \right]^{1/4}$$

P_{BH} fracture wall [Pa]

P_{init} = Viscosity of hot water [Pa·s]

       = Viscosity of cold water [Pa·s]

       = Bottom hole pressure [Pa]

       = Initial reservoir pressure [Pa]

$$(62) \quad P_{BH} = P_{init} + \Delta P_1 + \Delta P_2 + \Delta P_{face}$$

(Koning, 1988) used a one well approach and adopts a time dependent exterior radius (Re) in equation 63 and (Veldkamp, 2015) uses the distance between the injection and the production well. Re is the distance from the well that is affected by the change in pore pressure as a result of injection, and is dynamic in time. In a doublet system, a steady state pressure profile between the injector and producer is established after a certain period of time and therefore Re can be replaced by the distance between the two well. However, out tool is a one well approach as well, and therefore we use Re, which is defined as

$$(63) \quad Re = 1.5\sqrt{\kappa t}$$

In which t is time and κ is the hydraulic diffusivity of the reservoir, which can be derived from the permeability and porosity of the rock, the viscosity of the fluid and the total compressibility of the reservoir, as stated in equation 64.

$$(64) \quad \kappa = \frac{k}{\varphi \mu c_t}$$

Prior to fracture formation, the bottom hole pressure derived from equation 62, is similar to the pore pressure at the borehole wall calculated by the Theis function. The bore hole pressure required to overcome the tensile strength of the rock (Eq. 8), is referred to as the breakdown pressure of the formation and can be used to define the minimum horizontal stress of the reservoir in leak-off tests.
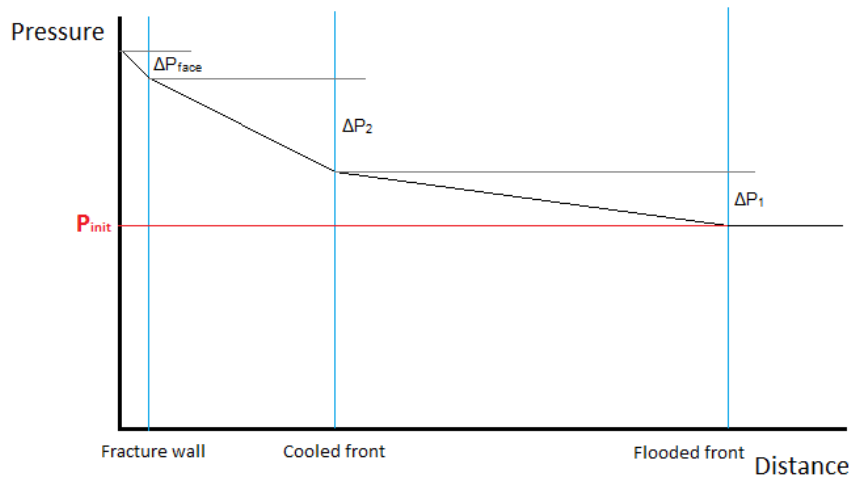
Figure 16: The borehole pressure is calculated by adding the pressure rises at the flooded front boundary, the cooled front boundary and at the fracture wall.

3.3.6 FRACTURE GROWTH & GEOMETRY

Defining the geometry of a hydrothermal fracture is a complex matter. The growth, in width and length, of fractures depends on the interaction of various processes; such as fluid flow within the fracture, leak-off to the formation and the evolution of stresses and pressures at the fracture tip. All these processes occur simultaneously, and finding the proper balance is challenging.

Bottom hole pressure as a result of fractures

Well stimulation changes the bottom hole well pressure. The opening of fractures decreases the resistance of fluids to flow into the formation. Therefore the injection rate increases without changing the total injection pressure. Thus, each time the fracture grows the resistance of fluids to flow into the formation increases and the pressure at the borehole drops. This effect can be included by adding the pressure change as a result of the skin factor (Eq. 11). By assuming that the net to gross ratio of the reservoir is 1, in other words by assuming that the quality of the reservoir is 100%, equation 11 becomes

$$(65) \quad \Delta P_{skin} = \frac{Q\mu_{cold}}{2\pi kh} Skin$$

The skin is negative for hydrothermal fractures and decreases with fracture length, which means a decrease in bottom hole well pressure as fractures grow. How the skin factor of the well is calculated is described in section **Fout! Verwijzingsbron niet gevonden.**.

$$(66) \quad P_{BH} = P_{init} + \Delta P_1 + \Delta P_2 + \Delta P_{face} + \Delta P_{skin}$$

Pressure at the fracture tip; linear pressure drop within a fracture

The fluid pressure at the wellbore is generally higher than the fluid pressure at the tip of the fracture. This is dependent on the fluid flow throughout the fracture, which is dependent on the fracture geometry, injection pressure and fluid viscosity. Fluid flow through fractures is described as steady state laminar flow between two smooth parallel plates. The linear pressure drop with distance from the injection source is solved for Newtonian fluids by the cubic law equation.

$$(67) \quad \Delta P_{frac} = \frac{12\mu Q}{w^3 h} L$$

In which w is the width of the fault, L is the length of the fracture, h is the height of the fracture, μ is the viscosity and q is the volumetric flow rate. In reality, the pressure drop is generally larger than calculated. This is because the walls of a fracture cannot be approximated by a smooth surface approach. In nature, fracture walls are characterized by bulges that may or may not result in contact asperities between the two surfaces. The roughness of the fracture surfaces complicates the fluid flow, by creating friction (*Figure 17*). (Louis, 1969) developed an empirical relationship to quantify friction. The pressure drop between the well bore and the extended fracture tip is then defined by multiplying equation 67 by the friction fracture of Louis (Eq. 68).
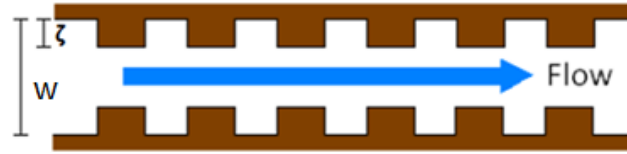
$$(68) \quad f_l = 1 + 3.1(\frac{\zeta}{w})^{1/5}$$

Figure 17: Side view of a fracture showing the relationship between fracture aperture and surface roughness (Civich, Unclear)

Fracture growth criterion

Fractures grow when the fluid pressure at the tip of the fracture overcomes the tensile strength of the rock at these locations (section **Fout! Verwijzingsbron niet gevonden.**), in other words if the net pressure becomes positive ($P_{net} = P_{tip} - \sigma_{h,tip}$). The total fluid pressure at the tip can simply be calculated by subtracting the pressure drop within the fracture from the total borehole pressure from equation 66.

$$(69) \quad P_{tip} = P_{BH} - \Delta P_{frac}$$

This pressure can then be used to calculate the poro-elastic stress changes of the surrounding rock, with the same formula as equation 55 for $\Delta\sigma_{bP}$. The temperature change at the extending end of the fracture might also be different from the temperature change at the well bore. The change in temperature is then calculated for the tip of the fracture using equations 19 to 26 in section **Fout! Verwijzingsbron niet gevonden.**. The total temperature change is then used to calculate the thermo-elastic stress changes at the fracture tip by equation 46 for $\Delta\sigma_{bT}$. The tensile strength of the extending part of the fracture can then be calculated; $\sigma_h = \sigma_{h,init} + \Delta\sigma_{bP} + \Delta\sigma_{bT}$. The net pressure at the fracture tip should always be smaller than zero, otherwise the fracture will grow. Fractures will then continue to propagate until this equilibrium is restored again (XX).

$$(70) \quad P_{net} = (P_{BH} - \Delta P_{frac}) - (\sigma_{h,init} + \Delta\sigma_{P,tip} + \Delta\sigma_{T,tip}) = 0$$

Fracture geometry

Once the tensile failure at the wellbore or the fracture tip is overcome the fracture starts to grow in width and in length. Rock, fluid mechanics and fluid loss considerations control the dimensions and geometry of the created fracture; such as the fracture height, length and width. Finding the balance between the width, length and the net pressure at the tip, can be done in several ways. Section **Fout! Verwijzingsbron niet gevonden.** already mentioned the three most widely used propagation models; the PKN, KGD and the radial model. This tool uses the PKN approximation, which assumes a constant fracture height as large as the confined reservoir height and assumes that the stresses in the cap and base rock are sufficient to prevent the fracture to grow out of the pay zone. Three methods to calculate the fracture dimensions are incorporated in the tool; an iterative method and the PKN approximation from (Economides M. N., 2000).

Iterative method

The iterative method solves the geometry problem by iterating over the fracture half-length until the net pressure at the fracture tip is zero. First the fracture width is determined by the expression of fracture width for PKN models from (Economides M. N., 2000).

$$(71) \quad w_{BH} = \left(\frac{\mu q L_f}{E'}\right)^{1/4}$$

With the symbols being
w_{BH} = Fracture width at the wellbore [m]
w_{av} = Average fracture width [m]
E' = plane strain modulus [Pa]

$$(72) \quad w_{av} = \frac{\pi}{5} w_{BH}$$

$$(73) \quad E' = \frac{E}{(1 - v^2)}$$

During each iteration, the pressure at the tip of the fault, as a result of fluid flow and friction, is calculated from equations 69. The tensile strength is also solved iteratively by defining the poro- and thermo-elastic stresses at the fracture tip for each fault length. The total fracture half-length is constrained when the pressure at the tip falls under the tensile strength. The same iteration starts again when the tensile failure criterion at the fracture tip is reached again.

PKN method

The breakdown of a formation and the fracture growth also exposes new formation area to the injected fluid and thus the leak-off rate into the formation starts to increase. However, if the pumping rate is maintained higher than the rate of leak-off into the formation, the fracture will continue to propagate and grow. The contribution of this leak of is therefore rather important. (Nordgren, 1972) improved the model previously defined by Perkins and (Kristianovitch, 1955), by adding the expression of material balance. He stated that at all times the volume that was injected into the well must be equal to the volume that leaked-off into the formation combined with the fluid volume stored in the fracture (Eq. 76).

$$(74) \quad V_i = qt$$

$$(75) \quad V_f = 2L_f h w_{av}$$

$$(76) \quad V_i = V_l + V_f$$

$$(77) \quad \eta = \frac{V_f}{V_i}$$

With the symbols being

V_i = injected fluid volume [m^3]
V_f = fracture volume [m^3]
V_l = leak-off volume [m^3]
H = fracture efficiency [-]

Nordgren (1972) initially obtained the solution for fracture growth numerically. However, two useful analytical approximations for the fracture geometry were derived for fractures of high and low efficiency. The efficiency of a fracture is a ratio between the volume stored in the fracture and the total injected volume (Eq. 77). The fracture has a low efficiency, when the fluid flow is dominated by leak-off into the formation, and the efficiency is high, when the fracture is storage dominated, i.e. when the fracture has a large volume. In general, when a fracture grows, it will shift from leak-off dominated to storage dominated once it has reached a certain size. The fracture geometry is then determined by the following equations.

Leak-off dominated ($\eta \rightarrow 0$)   Storage dominated ($\eta \rightarrow 1$)

$$(78) \quad L_f(t) = \frac{qt^{1/2}}{2\pi C_L h} \qquad\qquad (XX) \quad L_f(t) = 0.39 \left[\frac{E'q^3}{\mu h^4}\right]^{1/5} t^{4/5}$$

$$(79) \quad w(t) = 4 \left[\frac{\mu q^2}{\pi^3 E' C_L h}\right]^{1/4} t^{1/8} \qquad (XX) \quad w(t) = 2.18 \left[\frac{\mu q^2}{E'h}\right]^{1/5} t^{1/5}$$

Both solutions overestimate the fracture length and width (one of them neglects fluid loss and the other neglects storage), although according to (Economides M. N., 2000) the error is less than 10 percent. The parameter C_L is the leak-off coefficient. The size of this coefficient is dependent on the amount of fluid that is lost through the fracture and wellbore into the formation. How this can be obtained is described in section **Fout! Verwijzingsbron niet gevonden.**.
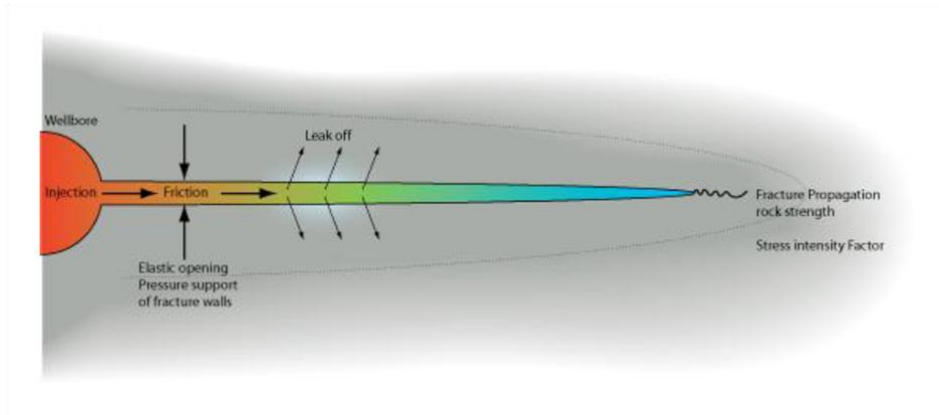
Figure 18: *Fracture propagation is a complex mechanism. The pressure and stress state at the tip of the fault is highly dependent on fluid flow and friction within the fault and leak-off to the formation.*

3.3.7 LEAK-OFF

Fluid that leaks from the fracture into the rock formation is referred to as fluid loss. In geothermal systems, this may occur through pre-existing fractures and pores or new fractures that are formed as a result of cooling of the rock (Ghassemi, 2003). Fluid loss is accounted for by two different mechanisms; storage loss and leak-off. Storage loss is the fluid that remains in the fracture and is used to determine the size of the fracture, and leak-off is considered the fluid that is lost to the surrounding porous medium through flow.

Propagating a fracture requires the minimum effective stress to be overcome at the tip of the fracture. However, while the fracture is propagating fluid leaks off into the formation before reaching the fracture tip (Bellarby, 2009). Thus, the longer the fracture, the more leak-off there will be, and the more injection pressure that is required for the fracture to continue growing. The rate of fluid that is lost to the surrounding formation is governed by the total leak-of coefficient (C_L). This value varies typically from 0.0005 to 0.05 ft./min$^{1/2,}$ which can be converted to m/day$^{1/2}$ by multiplying the value by 3.28/1440$^{1/2}$ (Economides, 2000).

The total leak off of a system is dependent on a combination of three flow resistant mechanisms that are encountered in fluid loss from the fracture (MFrac User's Guide, 2011). These mechanisms are: 1) the fracture fluid leak-off viscosity and permeability effect (C_V), 2) the reservoir viscosity and compressibility effect (C_C) 3) and the wall-building effects (C_W),. The total leak-off coefficient is very important, since it determines the geometry of your fracture.

Fluid loss is assumed to occur over the complete pay zone height and can be determined by the harmonic weighing of the leak off components (personal communication F. Pizzocolo (TNO), (MFrac User's Guide, 2011; Barree, 2009)).

(80) $\quad C_L = \dfrac{C_v C_C C_w}{C_v C_C + C_C C_w + C_v C_w} \;\; or \;\; \dfrac{1}{C_L} = \dfrac{1}{C_v} + \dfrac{1}{C_C} + \dfrac{1}{C_w}$

The three flow resistant effects are calculated with the following equations. C_V and C_C are both directly related to reservoir properties. Whilst injecting, the fracturing fluid must displace or compress the reservoir fluid to filtrate into the formation. Reservoirs that are easily compressible, or with low reservoir fluid viscosity, promote a greater leak-off. This effect is captured in the C_C component of the leak off coefficient. Secondly, as the fracturing fluid invades and displaces the fluid in the reservoir, this results in a pressure difference through the invaded zone due to fluid viscosity and relative permeability. This effect is represented by the C_V component. And last, fluid loss is defined by C_W, also referred to as the wall building or filter cake coefficient. Fluids can produce a wall on the fracture face by the deposition of filter-cake. Initially, when a fresh fracture wall is exposed, the filter cake is non-existent and fluid will be lost more easily to the surrounding formation. With the presence of filter-cake fluid flow is reduced and fluid travel more easily through the fracture. This effect is also called spurt loss and acts as a controlling factor of leak off.

(81) $C_V = 0.0469 \sqrt{\dfrac{K_f \Delta P \varphi}{\mu_f}}$

(82) $C_C = 0.0374 \Delta P \sqrt{\dfrac{k_r c_t \varphi}{\mu_r}}$

(83) $C_w = \dfrac{0.0164m}{A}$

With the symbols being:

K_f	= Effective fracturing fluid filtrate permeability [D]
k_r	= Reservoir permeability to reservoir fluid [D]
ΔP	= Differential leak off pressure [Pa]
ϕ	= Porosity [-]
μ_f	= Viscosity of fracturing fluid filtrate [Pa s]
μ_r	= Reservoir fluid viscosity [Pa s]
c_t	= Total formation compressibility
m	= Slope of volume versus square root of time plot [L/s]
A	= Cross-sectional area of fracture [m^2]

There is a limit as to how far a hydraulic fracture can propagate and leak-off plays an important role in this process. Leak-off increases for longer fractures, low permeability reservoirs and highly viscous reservoir fluids. Therefore, low permeability reservoirs benefit from longer hydraulic fractures than higher permeability ones.

3.3.8 WELL PRODUCTIVITY

Hydraulic fractures can increase the production of geothermal energy by creating a highly conductive connection between the wellbore and the reservoir. Productivity of a fractured well is a function of the reservoir drainage area – the flooded and cooled front -, the geometry and dimensions of the fracture, the fracture and formation conductivity and characteristics of any damage created during the process (Suri, 2010). The latter is a result of the water leak-off into the formation as described earlier.

The effect of hydraulic fractures on well production has been studied by many authors (Pratts, 1961), (Economides M. N., 2000) and (Egberts, 2001). Most of them present their results by plotting the productivity index J, normalized over a base productivity index J_0.

(84) $J_0 = \dfrac{2\pi kh}{\mu \ln(\frac{Re}{R_w})}$

J_0 is defined as the productivity index of an unstimulated well in a circular drainage area. Then J can be calculated by the change in bottom hole pressure and skin of the fracture

$$(85) \quad J = = \frac{2\pi k h}{\mu \ln\left(\frac{Re}{R_w}\right) + Skin}$$

The increased or decreased productivity of a well can then be obtained by J/J_0, and shows how much the pressure drop increases as a result of fracture formation with respect to an unstimulated well. This gives an insight in the potential to improve of the injection well by fracturing.

Skin

The skin of a stimulation treatment can be determined by using the final fracture length (Eq. 86). In this equation the constant G is taken to be the conductivity and it is equal to 0.69. According to (Detienne, 1998) the conductivity (G) of a fracture has an asymptotic value of 0.69 for conductivities relatively larger than 30, which is assumed to be valid for fractures of infinite conductivity.

$$(86) \quad Skin = G - \ln\left(1 + \frac{L_f}{R_{well}}\right)$$

3.4 MODEL VALIDATION

The hydrothermal fracture tool is validated by comparing its results to a confidential tool of TNO (Veldkamp J. L., 2015). Both models were run with, were possible, the same input parameters (**Table 2 & 3**). The stimulated reservoir lies at a depth of 4000 meter and has a thickness of 80 meter. The reservoir is relatively highly porous and permeable, with φ = 0.24 and k = 100 mD. The reservoir has an initial temperature of 120 °C. The elastic behaviour is characterized by a Young's modulus of 13.8 GPa and a Poisson's ratio of 0.24. Fluids are injected for a duration of 2 years, with and injection rate of 8000 m^3/d. The temperature of the injective is 30 °C.

Injection properties		
Parameter	**Unit**	**Value**
Injection rate	m^3/d	8000
Duration of injection	Days	730
Temperature of injective	°C	30
Density of injective	kg/m^3	1158
Viscosity of injective	Pa·s	0.0013
Heat capacity of injective	J/m^3 °C	3.817e6
Compressibility	1/Pa	4.4e-10
Salinity	mg/L	200.000

Table 1: Injection properties of the model. The blue values are calculated automatically by the tool.

Reservoir properties		
Parameter	**Unit**	**Value**
Thickness	M	80
Depth	M	4000
Radius of well	M	0.11
Permeability	mD	100
Porosity	-	0.24

Reservoir temperature	°C	120
Density of formation	kg/m^3	2300
Formation compressiblity	1/Pa	8.93e-7
Heat capacity of formation	J/m^3 °C	2.1e6
Heat capacity of cap/base rock	J/m^3 °C	2.1e6
Thermal diffusivity of cap/base rock	m^2/s	1.3e-6
Thermal expansion coefficient	°C^{-1}	1e-5
Biot's value	-	1
Young's modulus	GPa	13.8
Poisson's ratio	-	0.25
Density of formation fluid	kg/m^3	1104
Viscosity of formation fluid	Pa·s	0.000408
Heat capacity of formation fluid	J/m^3 °C	3.67e6
Leak off coefficient	m^2/√(day)	0.000045

Table 2: Reservoir properties of the model. The blue values are calculated automatically by the tool.

The results that came from the TNO tool are then compared with all three fracture methods developed in our tool; the iterative method, PKN method and Koning's method. The results can be found below.

3.4.1 RESULTS

The results are mainly focussed on the extent of the fracture during stimulation and the skin development of the well. **Figure 20** shows the fracture evolution for the iterative method and TNO's tool. TNO's tool calculated a fracture half-length of a little over 150 m, which is quite similar to the fracture length of 147 m derived from the iterative method. In both cases the fracture starts to grow a little after injection has started. However, the iterative method shows a higher propagation velocity in the beginning of injection and ceases when injection continues, whereas TNO's tool shows a fracture length that is approximately linear with time. According to (Economides M. N., 2000), it is safe to assume that the fracture half-length is proportional to the square root of time. This is similar to the curve of the iterative method. This means that it becomes harder to propagate the fracture in time, i.e. the longer the fracture, the harder it becomes to keep it growing.
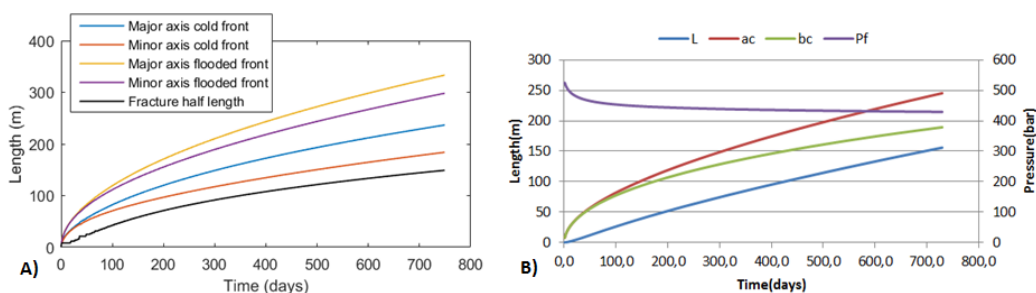

Figure 19: Fracture length comparison. Left) shows the fracture length in time of the iterative method and Right) the fracture length for the TNO's tool. Both plots show the evolution of the cooled and flooded front as well.

The model also ran for the propagation methods of PKN and Koning. The results are shown in **Figure 21**. It is obvious that these fractures do not propagate as far. To an extent of 110 meters for the PKN method and 66 meters for Koning. These methods both assume that the fracture length is dependent on the leak-off into the formation. If the leak-off rate, determined by the leak-off coefficient, is high, not all fluids will reach the fracture tip, when the fluids travel through the fracture. Therefore it is harder for the fracture to propagate. The fracture width also variates with each propagation method. Koning's method shows a fracture that has a small length and a relatively large average fracture width. Both PKN and the iterative method on the other hand show that the larger the fracture length, the smaller the fracture width. This makes sense for the iterative method, since the fracture width is proportional

to $L_f^{1/4}$. The width for the PKN method does not depend on the fracture length. However it does show a similar curve. They do assume that in the beginning of fracture formation the fracture propagation is mostly dominated by leak-off mechanism and this assumes thin fractures with little storage capacity.
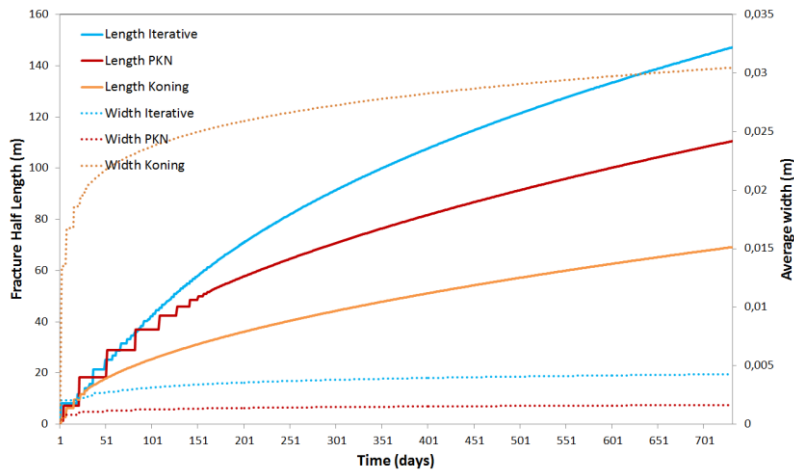

Figure 21: Fracture geometry of all three fracture propagation methods; the iterative method, PKN's method and Koning's method.

Fracture propagation also decreases the skin of the injection well by reducing the resistivity of the fluids to flow into the formation. The skin calculated by TNO's tool is shown in **Figure 22**. The skin reaches a value of -4.4 after 730 days of injection. The skin of our tool is quite a bit smaller though. It defines that after 730 years of injection the skin of the well is -6.5, -6.22 and -5.6 for the iterative, PKN and Koning method respectively (**Figure 23**). **Figure 23** also shows that the skin at the beginning of fracture propagation decreases significantly. When the fracture has propagated only a couple of meters, the skin of the well already drops to values of ~-3. This seems slightly exaggerated. This instantaneous decrease is skin however also causes a significant pressure drop at the well bore. With the result that the pore pressure at the fracture tip drops as well. This partly explains the step wise fracture growth at the beginning of fracture propagation. Once the fault propagates, the pressure drops as such that it takes a while to increase to the critical level again. This could perhaps be smoothened by smaller time-steps at the beginning of injection or a different definition of the well skin.
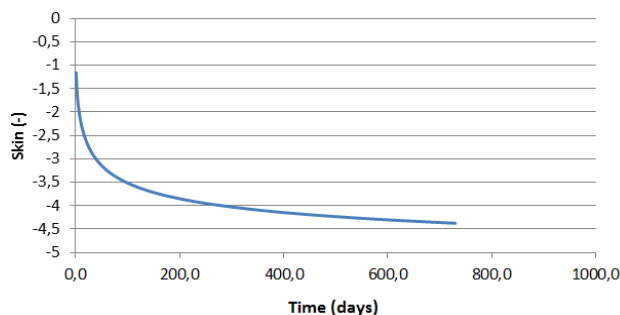
Figure 22: Well skin calculated by TNO's tool.

already drops to values of ~-3. This seems slightly exaggerated. This instantaneous decrease is skin however also causes a significant pressure drop at the well bore. With the result that the pore pressure at the fracture tip drops as well. This partly explains the step wise fracture growth at the beginning of fracture propagation. Once the fault propagates, the pressure drops as such that it takes a while to increase to the critical level again. This could perhaps be smoothened by smaller time-steps at the beginning of injection or a different definition of the well skin.

Figure 23 also shows the relative productivity index of the injection well. For each method, the productivity after injection is higher that the productivity before. For all cases the productivity

increases with a factor around 10. Obviously, the productivity increases the most for a larger fracture length and larger negative skin.
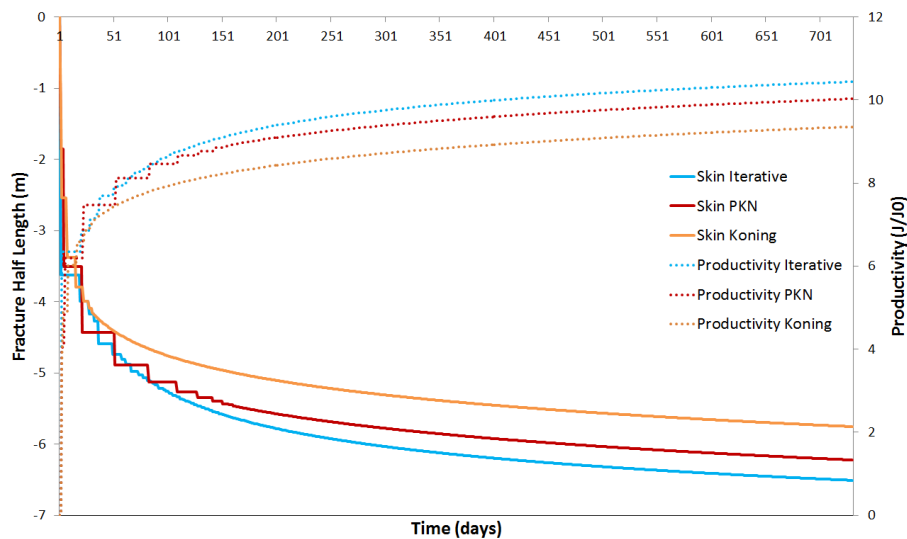

Figure 23: *The skin and productivity of the injection well.*

3.5 Sensitivity analysis

To determine which key parameters play the most important role in stimulation processes in geothermal fields, we executed a sensitivity analysis on the model results. Therefore we ran the model with a 10% deviation of the original input values given in **Table 2 & 3**. In other words, with a 10% decrease and a 10% increase. This was only done for the iterative method, since this one approximates the TNO tool the best, and for the PKN tool, since we are interested in the leak-off effect. The results are described below.

3.5.1 Results

Figure 24 shows the results of the sensitivity analysis for the iterative and PKN method in tornado plots. The effects of the key parameters on the fracture half length, the skin and the productivity of the well are determined.

The figure shows that the iterative method is mostly affected by the change in reservoir temperature (or injection temperature), the Young's modulus, the thermal expansion coefficient, the Poisson's ratio and the depth. These are all parameters that define the size of the stress change of S_h or that define the minimum horizontal stress itself. The depth is related to the minimum horizontal stress by the theory of Eaton (section **Fout! Verwijzingsbron niet gevonden.**). The shallower the reservoir, the smaller the overburden stress becomes and the smaller S_h. S_h decreases more than the initial pore pressure and one therefore needs less induced stresses to induce failure. For stiffer reservoirs, i.e. with a higher Young's modulus, the fracture propagates further. As can be seen from the figure, a 10% increase or decrease of the Young's modulus affects the outcome in a similar way as a 10% variation of the thermal expansion coefficient. This is a result of a linear relation of E and β with the thermo-elastic stress change. These stress changes are also proportional to the temperature change in the reservoir. The fracture half-length decreases significantly with decreasing reservoir temperature or increasing injection temperature. The Poisson's ratio, on the other hand, shows the opposite effect. A decrease in Poisson's ratio increases the fracture length and well productivity. All these parameters have a large effect on the thermos-elastic stress change, and therefore it can be stated that temperature does have a large effect on well stimulation. Thereafter, the injection rate, reservoir

thickness and heat capacity of the reservoir affect the fracture length. An increase in injection rate and a decrease in heat capacity and reservoir thickness increase the fracture length.
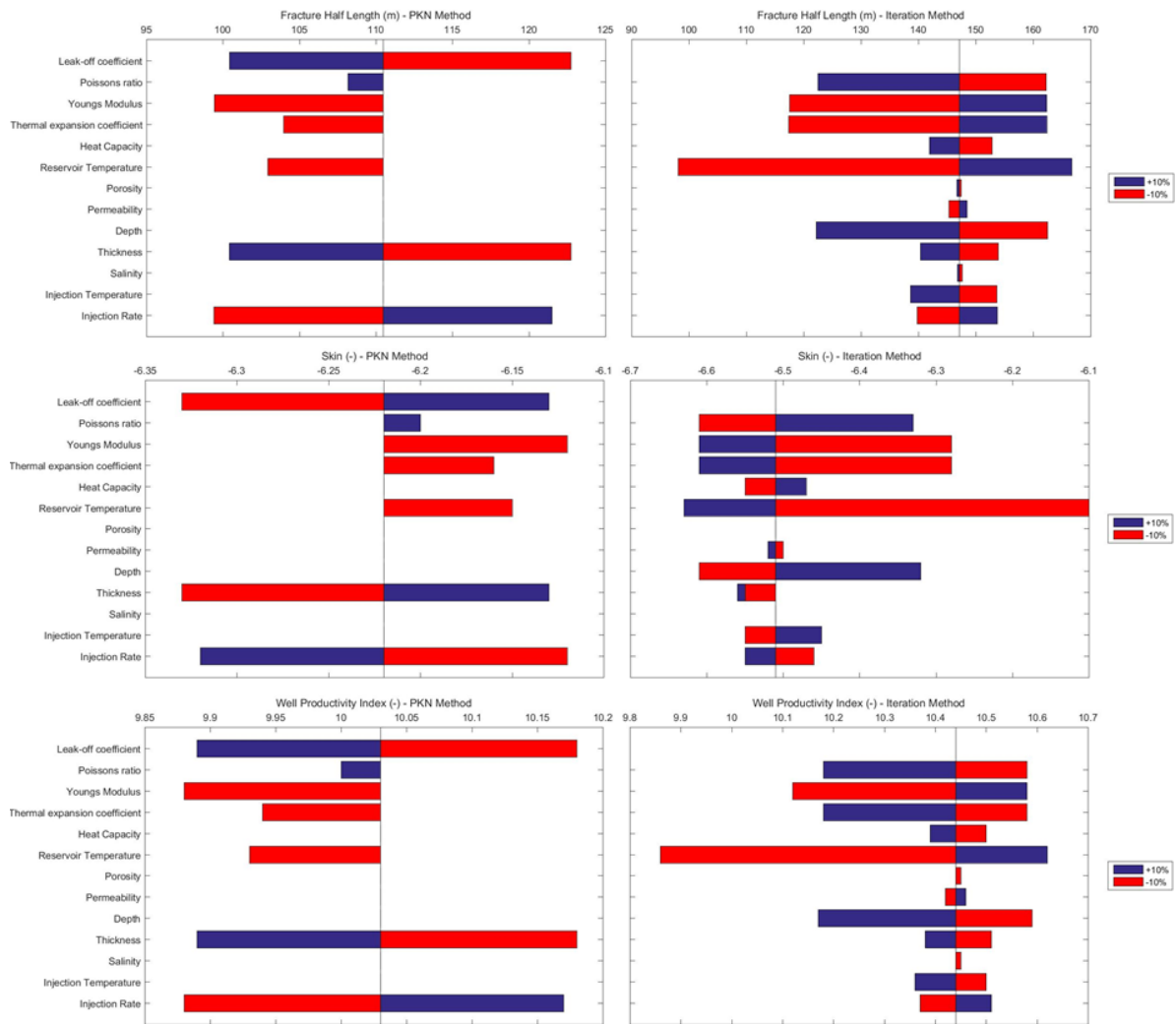
Figure 24: *Tornado plots of the PKN (left column) and iterative method (right column).*

The tornado plots for the PKN model look quite different. The fracture length of this model does not rely on the extent of the temperature front or the net pressure at the tip. However, the fracture length is highly dependent on the leak-off coefficient, the thickness of the reservoir and the injection rate. A higher injection rate means larger stress increases at depth and results in larger poro-elastic effects and fracture lengths. Similar to the iterative method, a smaller reservoir thickness leads to larger extending fractures. However, the effect on the PKN models is much higher.
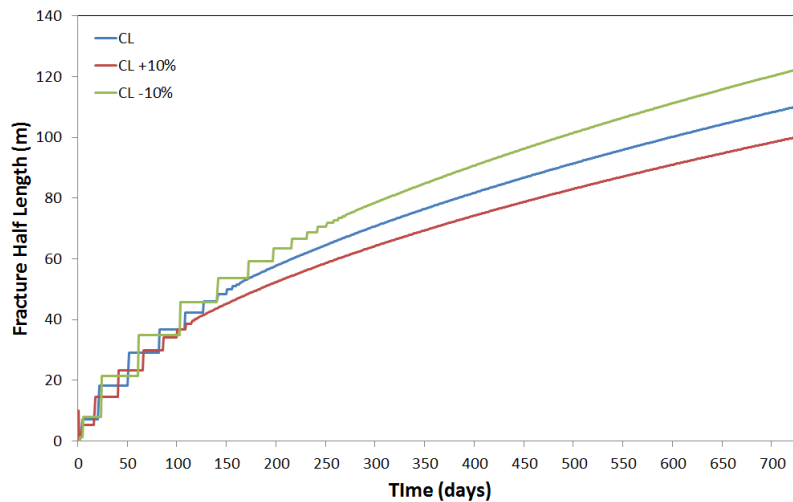
Figure 25: *The effect of leak off on fracture length. The higher the leak-off to the formation, the less fluid flows through the fracture and the smaller its dimensions.*

3.6 DISCUSSION & CONCLUSION

From the results described above, one can make several comments on the assumptions made in this hydrothermal stimulation tool. First of all, it is clear that, if one takes temperature effects into account, the thermos-elastic stress changes around the wellbore dominate over the poro-elastic stress changes, making it possible for fracture to form and grow. This effect is mostly significant in the vicinity of the well, whereas pressure changes take over at larger distances from the well as a result of the evolution of the cooled and flooded front. It is shown to be highly important for high enthalpy reservoirs, or reservoirs with a large temperature difference with the injective, for stiff reservoirs and for formations with large thermal expansion coefficients. Especially the first is highly applicable to (enhanced) geothermal systems and geothermal energy from volcanic regions.

For the iterative fracture propagation method, the sensitivity analysis points out that these parameters also highly affect the size of the formed fracture. A decrease in reservoir depth, and increase in Young's modulus, and increase in thermal expansion coefficient, an increase in temperature differential and a decrease in Poisson's ratio all result in an increase in fracture half-length and well productivity. The fracture growth is thus mostly affected by thermal processes. It is therefore highly recommended that one knows these site-specific parameters prior at the tip. However, the fracture length is highly dependent on the leak-off coefficient, the thickness of the reservoir and the injection rate. A higher injection rate means larger stress increases at depth and results in larger poro-elastic effects and fracture lengths. Similar to the iterative method, a smaller reservoir thickness leads to larger extending fractures. However, the effect on the PKN models is much higher. to reservoir development to obtain the best approximation for the treatment plan. Especially the thermal expansion coefficient shows large deviations in outcome, for relatively small changes in the coefficient. It is assumed that the value lies between 1e-5 and 1e-6 (Zoback, 2007), however changing the value throughout this range can mean the difference between no fracture and a fracture in the order over several hundreds of meters.

For the PKN model, the sensitivity analysis shows different important parameters. This fracture formation is more dependent on the injection rate, thickness of the reservoir and the leak-off coefficient. This states that the fracture length increases as a result of increasing injection rate, decreasing reservoir thickness and decreasing leak-off coefficient. The first two are also noticed to be important for the iterative method, however much less than the parameters that affect the thermal stresses. Thereby the leak-off has a large effect as well. This coefficient states how much fluid is lost to the formation before the fluid reaches the fracture tip. High leak-off rates then lead to small fractures or no fractures at all. The leak-off could be approximated for a reservoir from leak-off tests

and surely has a large effect on the poro-elastic stress changes at the fracture tip. Overall, we can state that the iterative method overestimates the fracture length, since it does not take into account leak off between the wellbore and the fracture tip. However the PKN model underestimates the fracture length, since it does not properly take into account the temperature effects at the fracture tip, since the analytical solution was derived only for the effects of pore pressure. The net pressure at the tip is from a certain point onwards positive and this should, in reality, never be possible.

The pressure and temperature distribution before fracture growth are assumed to be radial, which could be approximately right for homogeneous and isotropic reservoirs, but as soon as a fracture starts to grow it is rather difficult to determine the pressure and temperature distribution around the fracture. (Ge, 2009) and (Koning, 1988) define how the pressure and temperature change around the fracture during propagation. They solve the pressure and temperature distribution in an elliptical approximation. This should be rather easy to implement, but could not be accomplished during the time span of this study.

Another assumption that is not very realistic is the one of a radial infinite, homogeneous and isotropic reservoir. All real reservoirs are heterogeneous, either by lithostratigraphic layering or by the presence of boundaries, such as faults. These should be taken into account. Currently, we assume that the fracture forms over the whole thickness of the reservoir and propagates similar in the lateral direction for all depth, but in reality this is far from true. Also the temperature and pressure profile do not travel as simply as assumed by the cooled and flooded front. Including layers with different rock properties, or more complex pressure and temperature profiles with depth could help getting a better insight in the fracture formation.

Lastly, the well productivity increase is linearly related to the skin of the well. This skin is now determined by (Detienne, 1998). However, this approximation already shows a skin decrease to -3 for fracture lengths of a couple of meters. This highly affects the well productivity, but more than is assumed from field developments. Further research on the determination of the well skin is therefore recommended.

3.6.1 RECOMMENDATIONS

The hydrothermal stimulation tool gives a nice idea on how fractures develop and grow in geothermal reservoirs; however the tool is not perfect yet. With the discussion points, mentioned above, we would like to recommend some improvements to the tool.
- Include a leak off term to the iterative fracture propagation method to reduce the overestimation of the fracture length
- Determine how fractures develop in a layered reservoir
- Implement smaller time steps at the beginning of injection, to smoothen out the step wise fracture growth.
- Include the elliptical distribution of the pressure and temperature during fracture growth to see how it affects the rest of the reservoir.
- Include a better approximation of the skin of the well.

And a last recommendation is that the tool should be tested and validated on real field data. This was initially the idea, however, time wise and logistic wise this was not feasible. The tool was originally made to study the thermal effects in high enthalpy geothermal regions, such as Indonesia. This would mean rather shallow reservoirs, with high stiffness (volcanic rocks) and large temperature differences. ertainly areas that are interesting for hydrothermal stimulation. The following data should be retrieved from a successful treatment site; 1) Stress state magnitudes, 2) Well data, such as leak-off tests, well logs and other data from drilling activities, to define reservoir characteristics and temperatures, 3) seismic interpretations and data from seismic activity in the region and 4) Injective data, such as treatment schedules including injection rate, temperature and duration.

4 SUBSIDENCE & INDUCED SEISMICITY TOOLS

Geothermal energy production changes the in situ stresses in the subsurface. Subsequently, this has an impact on surface movement and fault (re)activation. The cooling of the rock due to injection, may lead to compaction of the reservoir, which accommodates land subsidence (section **Fout! Verwijzingsbron niet gevonden.**). The magnitude and distribution of subsidence depends on the elastic properties of the reservoir and the evolution of the cooled front within the subsurface. This cooled front also affects the stress states of the pre-existing faults in the reservoir. Stress paths of these faults can become critical as a result of temperature and pressure changes, and induce seismicity. These mechanisms raise safety concerns by an increased risk of water flooding and constructional damage - to houses and buildings as well as geothermal wells and operation equipment.

We developed two semi-analytical tools to obtain first order approximations of subsidence and seismicity risks during geothermal reservoir development; the compaction and subsidence tool and the induced seismicity tool.

- **Compaction and Subsidence Tool (CST):** The tool is capable of estimating the order of magnitude and extent of compaction and accompanying subsidence for a simple one layer homogeneous subsurface. The quick, predictive tool can be used by operators prior to reservoir development to explore the need for a more thorough investigation in depth.

- **Induced Seismicity Tool (IST):** This tool can be used to get an insight in the potential of fault reactivation due to injection. It is possible to model the temperature and pressure changes on a fault in time and predict their influence on the stress state of the fault; whether a fault will fail or not.

Knowledge about the risk and size of subsidence and/or fault reactivation is essential in geothermal reservoir management. It can be used to develop tailor made injection schedules to mitigate the risks on subsidence and/or seismicity related problems. This contributes to safety regulations and public acceptance of geothermal projects in the Netherlands. The theory and development of both tools are further discussed in this chapter.

4.1 MODEL SET-UP

Compaction and Subsidence Tool

The pressure and temperature changes within the reservoir due to fluid and heat flow, change the stress conditions in the subsurface. The elastic deformation in the reservoir due to the poro- and thermo-elastic effects are calculated based on the uniaxial compaction theory of Fjaer et al (2008), Geertsma (1973) and Brouwer et al (2005). Surface displacement is then derived from a relationship provided by Geertsma (1973) and is highly dependent on the depth of burial and the lateral extent of the reservoir. The relationship is based on a linear elastic, isotropic, homogeneous subsurface but more complex accurate estimations could be implemented by integrating over a multilayered overburden. The result is a subsidence profile at the surface for a compacting reservoir in a layered subsurface.

Induced Seismicity Tool

The induced seismicity tool uses the same approximation for the temperature, pressure and stress distribution as described in chapter 3. The poro- and thermos-elastic stress changes are used to determine the principal stresses at each location within the reservoir or on a pre-existing fault. The principal stresses can then be used to determine the shear stress and normal stress at each fault

point in time. This can be translated to a shear failure potential introduced by Soltanazadeh (2008) and Figuerido (2015). The result is a tool that determines the failure potential and stress path evolution on a fault within the reservoir.

4.2 GENERAL ASSUMPTIONS

The model is a simplistic reproduction of reality and therefore some important assumptions are made:
- Fluid flow and heat transport evolves radially outward from the injection well into the formation. This is approximated with the Lauwerier's solution and Theis function as described in section **Fout! Verwijzingsbron niet gevonden.**.
- The reservoir is assumed to be a laterally extending disk-shape within a elastically deforming half space; the nucleus-of-strain concept (section **Fout! Verwijzingsbron niet gevonden.**)
- Compaction in the reservoir is considered to be uniaxial, in other words deformation in the lateral direction is not included.
- The layers of the reservoir and overburden consist of linear elastic, homogeneous and isotropic rocks.
- The fault within the reservoir is assumed to be pre-existing and non-sealing. The pressure and temperature front flow right through it.
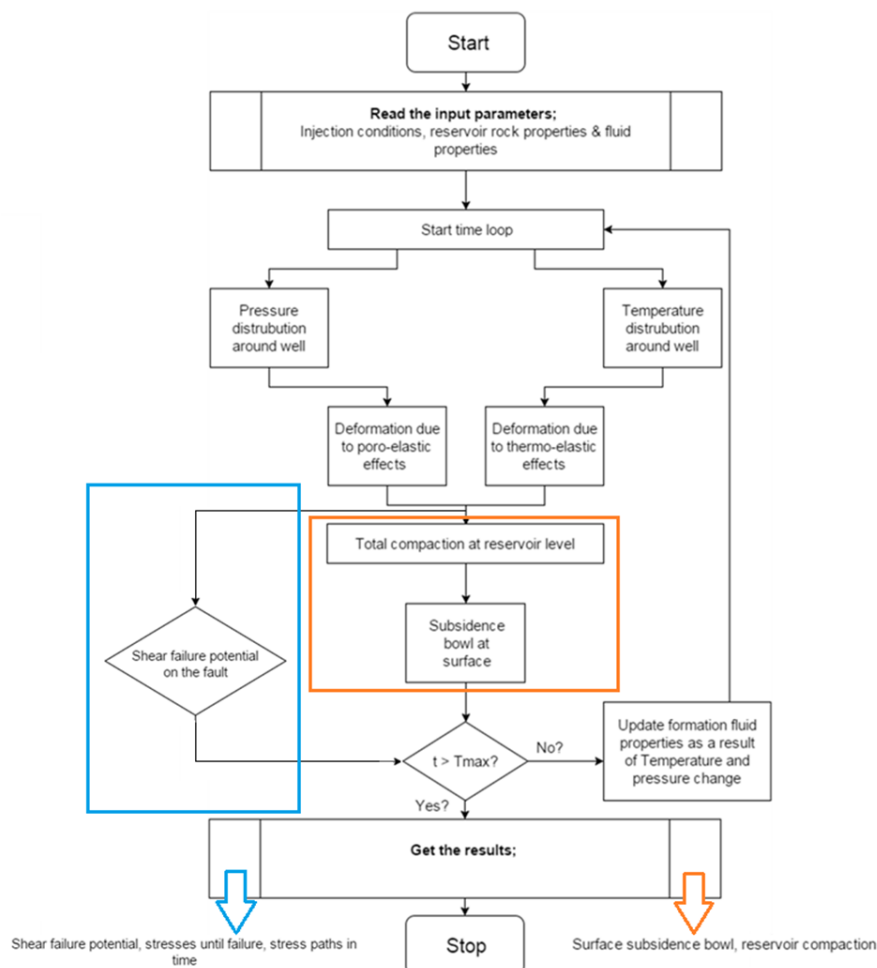
Figure 20 : *Flow charts of the risk assessment tools; the compaction and subsidence tool (orange) and the injection induced seismicity tool (blue).*

4.3 SIMULATION AND GOVERNING EQUATIONS

The method used the same expressions for the radial temperature and pressure distribution around the well bore as mentioned in section **Fout! Verwijzingsbron niet gevonden.** and **Fout! Verwijzingsbron niet gevonden.** for the hydrothermal fracking tool. Also the formation fluid characteristics are incorporated again, as described in section **Fout! Verwijzingsbron niet gevonden.**. New elements are the reservoir compaction due to P&T changes and the associated surface subsidence, and the theory of shear failure for fault reactivation. The complete flow chart of the tool is shown in **Figure 20**.

4.3.1 INDUCED STRESSES AND ASSOCIATED RESERVOIR DEFORMATION

Thermal expansion, or contraction or expansion due to pore pressure variations, have similar effects on the bulk stress-strain system (Brouwer, 2005). According to (Geertsma, 1973), the relationship between the two cases is:

$$(87) \quad \alpha \Delta P \;\leftrightarrow\; \beta_v K \Delta T$$

In which K is the bulk modulus defined by equation 90 and β_v is the coefficient of volume expansion, which is three times larger than the linear expansion coefficient (Eq. 88). This simply gives the ratio of change in volume per degree Celsius compared to the volume in the initial state.

By using the model of uniaxial compaction, the compaction of a reservoir due to depletion is calculated by expression 91. The expression shows that it is affected by the total reduction or increase in reservoir pressure, the vertical extent of the zone in which pore pressure change take place and lastly by the relevant deformation property of the reservoir rock. The latter is defined by the coefficient of uniaxial compaction, which is related to the vertical strain Δh/h and the pressure drop (Eq. 89). According to the theory of elasticity, the rebound caused by water injection will be equal to the subsidence caused production. In reality, this rebound is likely to be a fraction of the subsidence (Brouwer, 2005), however for simplicity our tool sticks to equal effects.

The reservoir deformation due to reservoir cooling can be estimated by equation 92. Since the temperature change is negative the change in height is negative as well, i.e. compaction. The thermal compaction due to thermo-elastic stresses is generally significantly higher than the compaction resulting from pore pressure reduction.

$$(88) \quad \beta_v = 3\beta$$

$$(89) \quad C_m = \frac{\Delta h}{h}\frac{1}{\Delta P} = \frac{1+\nu}{1-\nu}\frac{1-2\nu}{E}$$

$$(90) \quad K = \frac{E}{3(1-2\nu)}$$

With the symbols being:

β = thermal expansion coefficient [°C^{-1}]
β_v = Coefficient of volume expansion [°C^{-1}]
C_m = Coefficient of uniaxial compaction [-]
Δh = Deformation of reservoir [m]
Δh_P = Deformation due to poro-elastic effects [m]
Δh_T = Deformation due to thermo-elastic effects [m]
K = Bulk modulus [Pa]

(91) $\Delta h_P = h\, C_m \Delta P$

(92) $\Delta h_T = h\, C_m \beta_v K \Delta T$

E	= Young's modulus [Pa]
v	= Poisson's ratio [-]
ΔT	= Temperature change [°C]
ΔP	= Pressure change [Pa]

The total compaction or uplift of the reservoir can be obtained by simply adding Δh_P and Δh_T. Therefore, the part around the injection well will yield extensional stresses due to pore pressure increase that compensate some of the compressional stresses due to cooling. However, in the depleting part of the reservoir, around the producing well, temperature effects are negligible and compaction is only related to the decrease in pore pressure.

4.3.2 SUBSURFACE SUBSIDENCE

Compaction of the reservoir results in subsidence on the top of the reservoir and uplift of the bottom of the reservoir (**Figure 9**). The deformation at the top is larger than at the bottom since it can propagate more freely to the ground surface because the ground surface is unconstrained. Deformation in other directions, e.g. laterally, is therefore limited due to its constrained surroundings. If, according to (Geertsma, 1973), the compaction at the reservoir level is lower than 10 centimetres, there is little reason to pursue the matter further. However, is larger values are obtained, the subsidence at the surface should be clarified to establish any consequences. In order to see a considerable degree of subsidence, one or several of the following conditions must be present (Fjaer, 2008).

- The pressure drop due to production or the temperature change due to injection must be significant. Pressure maintenance by e.g. waterflooding could counteract compaction.
- The reservoir rock is highly compressible; compaction is more severe in soft rocks.
- The reservoir must have a considerable thickness.
- Subsidence is directly related to the amount of compaction at the reservoir level. It is also dependent on the overburden rock properties, such as depth, geometry and on the contrast in mechanical properties between the reservoir and its surroundings.

The nucleus-of-strain concept - a mathematical analysis first introduced by (Mindlin, 1950) and further improved by (Geertsma, 1973) - is capable of predicting how the deformation of a reservoir propagates through the overburden. The idea is to calculate subsidence resulting from the compaction of an isolated volume in the subsurface within a elastically deforming half-space with a traction free-surface (**Fout! Verwijzingsbron niet gevonden.**). The elastic moduli, C_m and v, are assumed to stay constant throughout the entire half-space, and in time as well. With this assumption, the subsidence above a disk-shaped reservoir can be found by integrating the nucleus solution over the entire reservoir volume. This results in a solution by equation XX and XX for vertical and horizontal deformation.
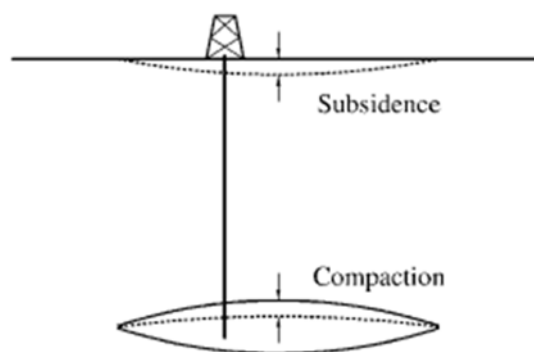
Figure 27: Reservoir compaction and surface subsidence (Fjaer, 2008). The reservoir is assumed to be an isolated, disk-shaped volume in a elastically deforming half space with traction free surfaces.

$$\frac{u_v(r,0)}{\Delta h_v(r,Z_{res})} = -2(1-v)A$$

$(93)\quad A = R_{res}\int_0^{\infty} e^{-Z_{res}\alpha}J_1(\alpha R_{res})J_0(\alpha r)\, d\alpha$

$$\frac{u_h(r,0)}{\Delta h_v(r,Z_{res})} = -2(1-v)B$$

(94)

$(95)\quad B = R_{res}\int_0^{\infty} e^{-Z_{res}\alpha}J_1(\alpha R_{res})J_1(\alpha r)\, d\alpha$

With symbols being:
$u_v(r,0)$ = Vertical displacement at surface [m]
$u_h(r,0)$ = Horizontal displacement at surface [m]
$\Delta h_v(r,Z_{res})$ = Vertical compaction at reservoir level [m]
Z_{res} = Depth of top of reservoir [m]
r = Distance from well [m]
R_{res} = Lateral extent of reservoir [m]
A = Dimensionless constant [-]
B = Dimensionless constant [-]
J_1 = First order Bessel function
J_0 = Zero order Bessel function

In which J_0 and J_1 are Bessel functions of the zero and first order respectively. This function is derived numerically within the tool, by using the besselj-function of Matlab. The tool gives the extent and size of the subsidence bowl over a compacting reservoir. The ratio of subsidence and the reservoir compaction is in essence determined by the ratio between the depth of burial and the lateral extent of the reservoir. Therefore, small, but deeply buried reservoirs are almost incapable of producing significant subsidence at the surface, even if their compaction at reservoir level cannot be neglected. On the contrary, large reservoirs at relatively large depths are potential candidates for subsidence. It is not commonly recorded though, since subsidence is less severe for low compaction coefficients, which are assumed to decrease with increasing effective stresses (and thus depth). However, the Slochteren gas field in Groningen, could for instance be a good candidate for surface subsidence. This reservoir has a significant thickness, has a large lateral extent, is relatively weakly consolidated and is buried at shallow depths. A more detailed investigation could be desirable in such cases.

4.3.3 FAULT REACTIVATION

Fault reactivation as a result of reservoir perturbations is expected within geothermal fields, as explained in section **Fout! Verwijzingsbron niet gevonden.**. Cooling of the reservoir and the increase in pore pressure may affect the principal stresses as such that failure occurs on a pre-existing fault surface (*Figure 21*). To evaluate the risk on fault reactivation for general scenarios, the Coulomb Failure Stress Change method, CFS, has been developed (Soltanzadeh, 2008). This is defined as follows:

$(96)\quad CFS = \tau - \mu\sigma'_n$

Where τ is the shear stress on the fault and σ'_n is the effective normal stress on the fault zone, calculated by equation 11 and 12 from the largest compressive stress σ_1 and the minimum

compressive stress σ_3. $\mu\sigma'_n$ is also known as the critical shear stress (Eq. 13). In this expression, a fault within the reservoir is reactivated is CFS is greater than zero. The stress changes due to differential compaction is more complex (section **Fout! Verwijzingsbron niet gevonden.**), and is for now not incorporated in the tool.
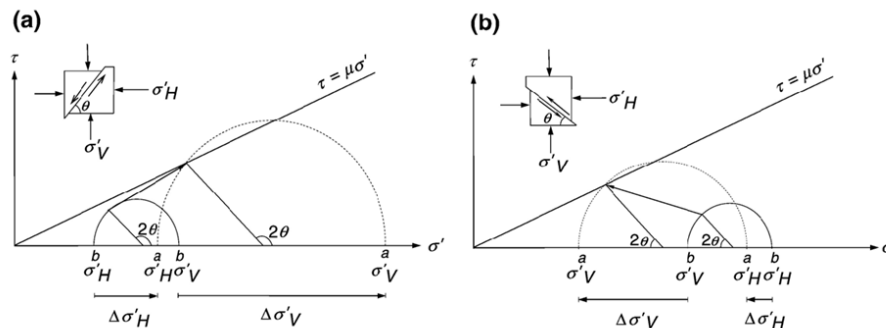

Figure 21: *Mohr-circle representation of stress changes resulting in fault reactivation for A) a normal fault within a reservoir during depletion and B) a thrust fault within a reservoir during injection. Index a denotes after change in pore pressure, and b denotes before.*

The potential for fault slip may also be expressed in terms of the fluid pressure required to induce slip. The maximum sustainable injection pressure then becomes, or critical pressure can be calculated from expression 96 as $P_c = \sigma_n - \tau/\mu$ ((Figueiredo, 2015). Figueiredo (2015) also states that when considering a Mohr-Coulomb representation of the fault, the potential of shear slip can be evaluated in terms of effective stresses

(97) $\sigma'_1 = S + q\sigma'_3$

In which S is cohesion and q is the slope between the effective principal stresses, which is related to the internal friction coefficient (Zoback, 2007).

(98) $q = \left[\sqrt{(\mu^2 + 1)} + \mu \right]^2$

If we then assume a value of the internal friction of 0.6 and zero cohesion for pre-existing fault, q becomes three ($\sigma'_1 = 3\sigma'_3$). This implies that shear slip is induced whenever the effective minimum principal stress is three times as small as the effective maximum principal stress. The critical pore pressure to induce failure then becomes

(99) $Pc = \dfrac{3\sigma_3 - \sigma_1}{2}$

4.4 RESERVOIR TOOL VALIDATION

We validated the model by comparing compaction and subsidence results from our tool with results from the reservoir model of (Fokker, 2015). They formulated a reference case that is typical for greenhouse farmers in the Netherlands who are using geothermal heat directly for their operations (van Wees, 2012). The case applies to a reservoir at 2 kilometres depth with a thickness of 100 meter. The injection well injects fluids with 4800 m^3/d into a high permeable poro-clastic reservoir with a porosity of 20 percent. The injection pressures stayed constant after injection is initiated and continuous for 100 years. The injected water has a temperature of 30 °C and the reservoir has an initial temperature of 85 °C. The density, viscosity and heat capacity of the injective and reservoir

Reservoir properties		
Parameter	Unit	Value
Thickness	M	100
Depth	M	2000
Radius of well	M	0.11
Diameter of reservoir	M	1500
Permeability	mD	200
Porosity	-	0.20
Reservoir temperature	°C	85
Density of formation	kg/m^3	2700
Formation compressiblity	1/Pa	4e-7
Heat capacity of formation	J/m^3 °C	2.1e6
Heat capacity of cap/base rock	J/m^3 °C	2.1e6
Thermal diffusivity of cap/base rock	m^2/s	1.3e-6
Thermal expansion coefficient	°C^{-1}	1e-5
Biot's value	-	1
Young's modulus	GPa	9
Poisson's ratio	-	0.35
Density of formation fluid	kg/m^3	1027
Viscosty of formation fluid	Pa·s	0.000459
Heat capacity of formation fluid	J/m^3 °C	3.97e6

fluids are calculated by the theories described in section **Fout! Verwijzingsbron niet gevonden.** and the salinity is assumed to be constant through time and is kept at 70.000 mg/L. Other input parameters are described in **Fout! Verwijzingsbron niet gevonden.** and **Fout! Verwijzingsbron niet gevonden.**.

Table 4: Injection properties of the model. The blue values are calculated automatically by the tool.

Injection properties		
Parameter	Unit	Value
Injection rate	m^3/d	4800
Duration of injection	yrs	100
Temperature of injective	°C	30
Density of injective	kg/m^3	1052
Viscosity of injective	Pa·s	0.000958
Heat capacity of injective	J/m^3 °C	4.02e6
Compressibility	1/Pa	4.4e-10
Salinity	mg/L	70.000

Table 5: Reservoir properties of the model. The blue values are calculated automatically by the tool.

All models consider a one-way coupling in which the changed pressure and temperature fields directly influence the stresses and displacements. (Fokker, 2015) calculated the subsidence effects by using the semi-analytical approach of (Fokker P. O., 2006). There model is capable of including some basic geologic features such as layering of the subsurface. They compared their results with results of the analytical model of Geertsma for a homogeneous subsurface, over a layered reservoir (Geertsma, 1973).

4.4.1 RESULTS

For the field case described above, we calculated the radial distribution of temperature and pressure within the reservoir. The progressive cooling and flow is shown by the curves in **Fout! Verwijzingsbron niet gevonden.**, which shows that the temperature and flooded front move outward from the injection well. Vertical reservoir deformation as a result of injection is shown in **Fout! Verwijzingsbron niet gevonden.**. This figure shows that the maximum amount of compaction within the reservoir is approximately 22 cm. The effect of a pressure increase is well shown in the near well area. Here compaction is slightly smaller than in the surrounding rock. The elevated pressure in that region compensates the shrinkage of rock due to cooling. However, it is clear that the pressure effects are only locally detected and approximately only 10% of the thermal effects.
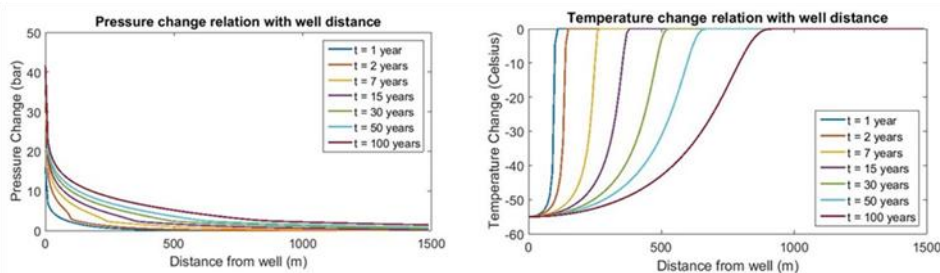

Figure 29: *Pressure (left) and temperature (right)distribution around the well for various times.*
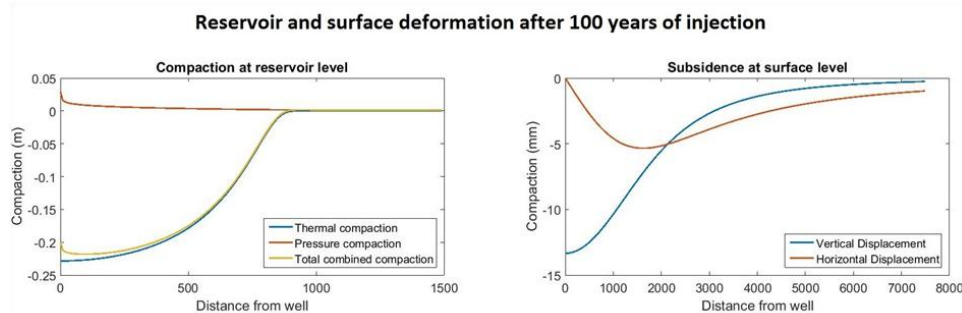

Figure 30: *Left) The compaction/uplit curves of the reservoir as a result of poro- and thermo-elastic stress changes. Right) The corresponding surface subsidence deformation.*

The total vertical compaction results were used as input for the subsidence calculations. We used a homogeneous overburden with the same elastic properties as the reservoir rock. This resulted in the horizontal and vertical displacement curves as shown in the left plot of Figure 30. The subsidence bowl reaches it maximum depth just above the injection well, where the surface falls with 13.3 mm over a time span of 100 years. The subsidence does affect and area much larger than the compacted area of the reservoir. An area of more than 154 million m2 is affected above the surface compared to an absolute compaction of 1.77 million m2 at the reservoir level.

The rate of subsidence is actually more interesting than the total surface movement. It is the acceleration of ground movement that does the most damage to infrastructure. We compared the maximum surface subsidence in time of our tool to the rate of subsidence obtained from the tool of TNO and the method of Geertsma (Fokker P. V.-D., 2015). This is shown in Figure 31. It is interesting to see that the subsidence rate of TNO and Geertsma is rather linear through time, whereas our tool has a logarithmic dependence on time. The rate of subsidence is significantly high as injection is initiated but decreases with ongoing injection. The tool of TNO includes a heterogeneous subsurface with and increasing Young's modulus with depth, whilst Geertsma holds a homogeneous subsurface.

The heterogeneous subsurface accommodates more surface subsidence than the homogeneous subsurface. The total subsidence calculated by our model falls in between the estimation by TNO and Geertsma.

properties as the reservoir rock. This resulted in the horizontal and vertical displacement curves as shown in the left plot of **Fout! Verwijzingsbron niet gevonden.**. The subsidence bowl reaches it maximum depth just above the injection well, where the surface falls with 13.3 mm over a time span of 100 years. The subsidence does affect and area much larger than the compacted area of the reservoir. An area of more than 154 million m^2 is affected above the surface compared to an absolute compaction of 1.77 million m^2 at the reservoir level.

The rate of subsidence is actually more interesting than the total surface movement. It is the acceleration of ground movement that does the most damage to infrastructure. We compared the maximum surface subsidence in time of our tool to the rate of subsidence obtained from the tool of TNO and the method of Geertsma (Fokker P. V.-D., 2015). This is shown in **Fout! Verwijzingsbron niet gevonden.**. It is interesting to see that the subsidence rate of TNO and Geertsma is rather linear through time, whereas our tool has a logarithmic dependence on time. The rate of subsidence is significantly high as injection is initiated but decreases with ongoing injection. The tool of TNO includes a heterogeneous subsurface with and increasing Young's modulus with depth, whilst Geertsma holds a homogeneous subsurface. The heterogeneous subsurface accommodates more surface subsidence than the homogeneous subsurface. The total subsidence calculated by our model falls in between the estimation by TNO and Geertsma.
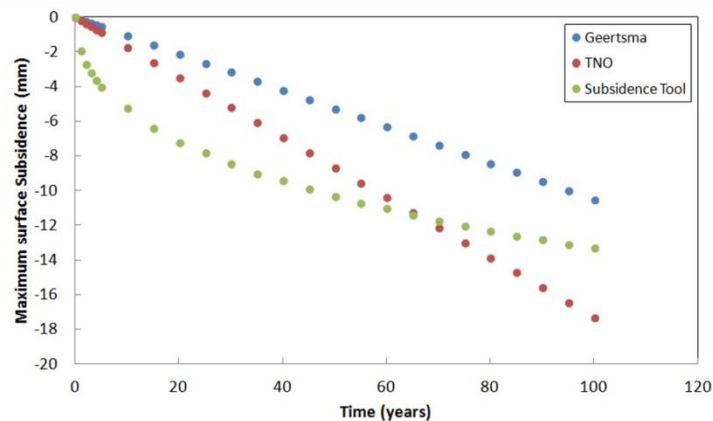

Figure 31: *Temporal development of the deepest value of subsidence for our tool, the tool from TNO and Geertsma's method. The last two are obtained from (Fokker P. V.-D., 2015).*

The potential for fault reactivation is analysed as described in section **Fout! Bladwijzer niet gedefinieerd.Fout! Verwijzingsbron niet gevonden.**. First we determined the area around the well that is prone to shear failure. Therefore we took normal faults with a dip angle of 60° and fault orientation with respect to the principal stresses is not taken into account. All faults are thus assumed to be orientated critically with respect to the minimum horizontal stress, which would be perpendicular to S_h, and this therefore shows the worst case for fault reactivation. The friction coefficient is taken to be 0.6. **Figure 22** shows the poro- and thermo-elastic stress changes within the reservoir, the injection well is located at zero point of the x-axis. Taking into account the fault properties and changes in effective stresses on the fault this leads to a radius of 668.5 meter, for which the failure stress is critical, i.e. CFS > 0. Perfectly orientated faults within this zone will shear.
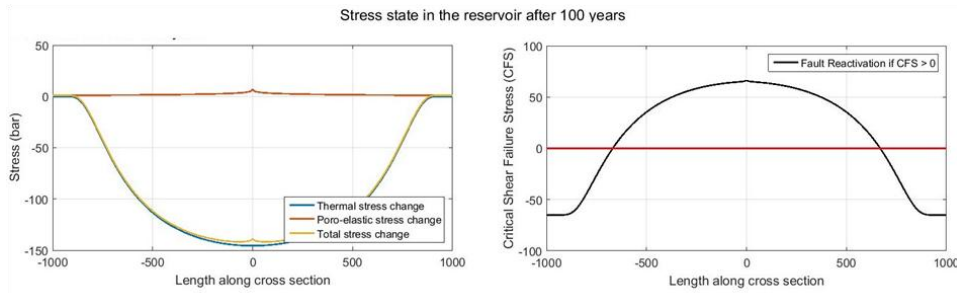
Figure 22:

To illustrate how the effective stresses on a fault change in time, we represented the stress paths of some normal faults in time. The faults are located at a different location from the injection well; at 100, 250, 500 and 1000 meter. The results are shown in **Fout! Verwijzingsbron niet gevonden.**. The thermo- and poro-elastic stress changes were calculated for the fault inside the reservoir and one assumed that the temperature and pressure front could easily propagate through the fault, in other words the fault is permeable and non-sealing.

Since the reservoir is quite permeable and has a high porosity, the pressure only increases with a couple of bars at the fault at the end of injection (right plot of **Figure 22**). Compared to the total pore pressure in the reservoir, this so significantly small, that a shift of the stress path to the left is not really visible. Thereby, the stress change due to the temperature change causes a decrease in horizontal stress of approximately 130 bars in the near well area. It can be stated that the temperature effects are the dominant triggering effect for shear failure in this case. All faults, except for the one at a distance of 1000 meter, will fail in shear, however, at different times. This is dependent on the time at which the temperature front arrives at the fault.
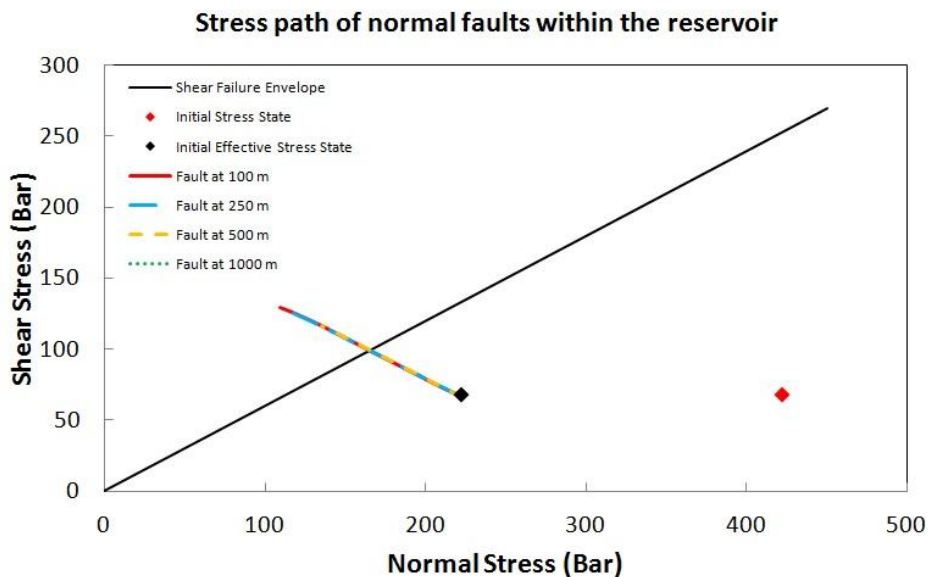

Figure 33: *Stress paths for normal faults at different locations of the injection well; 100, 250, 500 and 100 meter. Failure will occur on all faults except the one at a distance of 1000 meter.*

4.5 DISCUSSION & CONCLUSION

The risk assessment tool is capable of approximating the stress changes due to cooling and pore pressure increase around an injection well. The distribution of pressure and temperature is assumed to travel radially outward from the injection well. As already mentioned in the previous chapter, this is not very applicable for natural reservoirs. Natural reservoirs are more heterogeneous, due to for instance layering or due to fracture cross-cutting the reservoir. The permeability and porosity of the reservoir can also decrease in time as a result of pore closure during compaction. The estimation of the compaction at the reservoir level is therefore highly overestimated. The whole reservoir is assumed to be one homogeneous layer, and all displacement in the reservoir is in the vertical direction at the top of the reservoir. The same is done for the overburden. The deformation at the surface level shows vertical displacement and horizontal displacement. This horizontal displacement is largest near the well bore, since it has to compensate for the subsiding surface, i.e. it fills up the "voids". The relationship is based on a linear elastic, isotropic, homogeneous subsurface but more complex accurate estimations could be implemented by integrating over a multilayered overburden and reservoir. This would already include horizontal displacement at the reservoir level, as is expected. The result is a subsidence profile at the surface for a compacting reservoir in a layered subsurface.

Our subsidence model shows similar values of total vertical displacement at the surface as the model of (Fokker P. V.-D., 2015) and (Geertsma J. , 1973). However, the rate at which the subsidence is applied is linear for their models whilst our model shows a very high subsidence rate at the beginning of injection which decreases with time. It is not entirely clear why our model shows these results, however it could be a result of using one layer. All deformation at the reservoir level is in our case vertical, whilst both other models use an integration over the reservoir depth and therefore already a part of the deformation is translated into horizontal movement in depth.

The subsidence at the reservoir level is in between the 10 and the 17 mm. According to (Geertsma J. , 1973), there is no reason to pursue the matter any further if the reservoir compaction is lower than 10 cm. However, the compaction calculated with our model shows a compaction of 22 cm. Even though, this a large overestimation of the actual compaction, further, more detailed research is necessary to eliminate the risk on damaging surface subsidence.

The failure tool shows that all normal faults within a range of 668.5 meter from the injection well will shear. The stress paths of all fault points show that the pressure and temperature front travel in exact the same way through the different fault points at different times. This is not very likely to happen in nature, were the fluids travel through fluid pathways that are normally a little more complex than linear flow. Using a better software tool to estimate the temperature and pressure distributions around the well is therefore more encouraged. With these P&T distributions one can then calculate the critical shear failure potential at various locations. This could also be done for other types of faults, such as reverse faults or strike-slip faults.
Another assumption of the failure model is that the faults within the reservoir are fully permeable, i.e. the fault are not sealing, not for fluids and also nog for temperature. In natural fields, reservoirs are often bounded by sealing faults. These bounding faults can induce reservoir arching, as described in section **Fout! Verwijzingsbron niet gevonden.**, due to the effect that the horizontal and vertical stresses do not change with the same rate. This reservoir arching causes stress changes at the edges of reservoirs, at faults or in the sealing layers, which can result in induced seismicity. According to literature, (Segall, 1998) (Soltanezadeh, 2008), this is actually the largest contributing factor to induced seismicity. Stress arching is also highly applicable to high enthalpy reservoirs, since the large temperature differential induces a large decrease in horizontal stresses that also affect the reservoir boundaries. Contraction near the well pulls all connected rock mass towards itself and this can cause dilation at the bounding fault. This dilation can then result in shear failure. A study on the effects on reservoir arching is therefore highly recommended for geothermal reservoirs.

4.5.1 RECOMMENDATIONS

In order to improve the risk assessment tool a couple of mechanisms should be included:

- Heterogeneous distribution of pressure and temperature through the reservoir
- Calculation of compaction at the reservoir integrated over the total reservoir height. This results in horizontal and vertical displacement at the reservoir (instead of only vertical), and decrease the overestimation of surface subsidence.
- Include layering in the overburden. Deep reservoirs cannot be overlain by one homogeneous overburden. The various lithostratigraphies affect the total subsidence at the surface and also its lateral extent.
- A porosity decrease within the reservoir as a result of compaction. Fluids flow should become more challenging with ongoing compaction.
- Injection induced seismicity due to reservoir arching should be implemented. Some literature on this topic is from (Figueiredo, 2015) (Fokker P. V.-D., 2015) (Hassanzadegan, 2011) (Soltanzadeh, 2008) (Segall, 1998)

5 REFERENCES

Abé, H. M. (1976). Growth rate of a penny shaped Crack in hydraulic fracturing of rocks. *J. Geophys. Res. , 81*.

Adams, J. B. (2002). Equations of state for basin geofluids; algorithm review and intercomparison for brines. *Geofluids , 2*, 257-271.

Allen, D. (1968). Physical Changes of Reservoir Properties caused by Subsidence and Repressurizing Operations, Wilmington Field, California . *Journal of Petroleum Technologies* , 23-29.

Altmann, J. M. (2010). Poroelastic contribution to the reservoir stress path . *International Journal of Rock Mechanics & Mining Sciences , 47*, 1104-1113.

Baisch, S. V. (2006). Induced Seismicity during the stimulation of a geothermal HFR reservoir in Cooper Basin, Asutralia. *Bulletin of the Seismological Society of America , 96* (6), 2242-2256.

Barree, R. (2009). *Modeling of Frac-Fluid Rheology and Leakoff (Presentation) .* Barree & Associates .

Batzle, M. W. (1992). Seismic properties of pore fluids . *Geophysics , 57* (11), 1396-1408.

Bellarby, J. (2009). *Well Completion Design* (1st edition ed.). Hungary : Elsevier; Developments in Petroleum Science Volume 56 .

Biot, M. (1941). General theory of three-dimensional consolidations. *Journal of Applied Physics , 12*, 155-164.

Brady, B. (1992). *Cracking rock: Progress in fracture treatment design.* Schlumberger Oilfield Review.

Brouwer, G. L. (2005). Geothermal Heat and Abandoned Gas Reservoirs in the Netherlands . Antalya, Turkey: Proceedings World Geothermal Congress 2005.

Civich, W. (Unclear). *Chemical Engineering Research Project .* Australia : PIRSA.
Cladouhos, T. P. (2010). Injection induced seismicity and geothermal energy. *GRC Transactions , 34*, 1213-1220.

Economides, M. N. (2000). Reservoir Stimulation. In Schlumberger (Red.). England : Wiley & Sons Ltd.

Economides, M. O. (2002). *Unified Fracture Design; Bridging the gap between theory and practice.* Alvin, Texas : Orsa Press .

Egberts, P. F. (2001). A new analytical approximation for flow into a well in a finite reservoir. *Transport in Porous Media , 44*, 85-107.

Ellsworth, W. (2013). Injection induced Earthquakes. *Science , 341*, 142-149.
Feistel, R. M. (2007). A Gibbs-Pitzer function for high salinity seawater thermodynamics. *Progress in Oceanography , 74*, 515-539.

Fetter, C. (2001). *Applied hydrogeology* (4th ed. ed.). Upper Saddle River, New Jersey: Prentice Hall, Inc. .

Figueiredo, B. R. (2015). Coupled hydro-mechanical processes and fault reactivation induced by CO2 injection in a three layer storage formation. *International Journal of Greenhouse Gas Control , 39*, 432-448.

Fjaer, E. (2008). *Petroleum Related Rock Mechanics* (Developments in Petroleum Science 53 ed.). Amsterdam, Netherlands: Elsevier.

Fokker, P. O. (2006). Semi-Analytic Modelling of Subsidence. *Mathermatical Geology* , 565-589.

Fokker, P. V.-D. (2015). Surface Movement Induced by Geothermal Well Doublet. Melbourne, Australia : Proceedings World Geothermal Congress 2015.

Ge, J. (2009). *Modeling and Analysis of Reservoir Response to Stimulation by Water Injection.* Texas : A&M University .

Geertsma, J. d. (1969). A rapid method of predicting width and extent of hydraulically induced fractures. *SPE Journal of Petroleum Technology , 21* (12), 1571-1581.

Geertsma, J. (1973). Land Subsidence Above Compacting Oil and Gas Reservoirs. *Journal of Petroleum Technology SPE-AIME* , 734-744.

Ghassemi, A. (2003). *A Thermoelastic Hydraulic Fracture Design Tool for Geothermal Reservoir Development.* Grand Forks, ND : University of North Dakota .
Grunberg, L. (1970). Properties of sea water concentrates. (pp. 31-39). 3rd International Symposium on Fresh Water from the Sea.

Hassanzadegan, A. B. (2011). Induced Stress in a Geothermal doublet System. Standford, California : 36th Workshop on Geothermal Reservoir Engineering .

Healy, J. R. (1968). The Denver Earthquakes. *Science , 161*, 1301-1310.

Jaeger, J. C. (2007). *Fundamentals of rock mechanics* (4th ed.). Blackwell Publishing Ltd.

Koning, E. (1988). *Waterflooding Under Fracturing Conditions* . TU Delft .

Kristianovitch, S. Z. (1955). Hydraulic Fracture of an Oil-bearing Bed. *OTN , 5*, 3-41.

Kruseman, G. d. (1994). *Analysis and evaluation of pumping test data* (2nd ed. ed.). ILRI publication.

Louis, G. (1969). A Study of Groundwater in Jointed Rocks and its Influence on the Stability of Rock Masses. *Rock mechanics research, Rep 10* , 99.

Lubinski, A. (1954). Theory of elasticity for porous bodies displaying a strong pore structure. (pp. 247-256). Universty of Michigan: Presented at the 2nd US National Congress of Applied Mechanics.

Majer, E. B. (2007). Induced seismicity associated with Enhanced Geothermal Systems. *Geothermics , 36* (3), 185-222.

McGarr, A. (2002). Case histories of induced and triggered seismicity. In W. K. Lee, *International handbook of earthquake and engineering seismology* (p. 647).

MFrac User's Guide. (2011). *Meyer Fracturing Simulations User's Guide* (9th edition ed.). USA: Meyer & Associates, Inc.

Mindlin, R. C. (1950). Thermo-elastic stress in the semi-infinite solid. *Journal of Applied Physics , 21*, 931.

Mulders, F. (2003). *Modelling of stress development and fault slip in and around a producing gas reservoir.* Proefschrift TU Delft .

Nordgren, R. (1972). Propagation of a vertical hydraulic fracture. *SPE Journal , 12* (4), 306-314.

Orlic, B. (2009). Some Geomechanical Aspects of Geological CO2 Sequestration. Goa, India: The 12th International Conference of IACMAG.

Orlic, B. T. (2011). Assessing the integrity of fault-and top seals at CO2 storage sites. *Science Direct , 4* (Energy Procedia), 4798-4805.

Orlic, B. W. (2013). A Study of Stress Change and Fault Slip in Producing Gas Reservoirs Overlain by Elastic and Viscoelastic Caprocks. *Rock Mech Rock Eng , 46*, 421-435.

Perkins, T. G. (1985). The Effect of Thermoelastic Stresses on Injection Well Fracturing . *Society of Petroleum Engineers Journal* , 78-88.

Perkins, T. K. (1961). Widths of hydraulic fractures. *SPE Journal of Petroleum Technology , 13* (9), 937-949.

Pizzocolo, F. J. (2016). Temperature effects during injection in fractured reservoir. Bandung, Indonesia: TNO.

Pratt, W. J. (1926). Local Subsidence of the Goose Creek Field. *Journal of Geology , 34*, 577.

Pratts, M. (1961). Effect of vertical fractures on reservoir behaviour - Incompressible fluid case. *SPE Journal , 1* (2), 105-118.

Raleigh, C. H. (1976). An experiment in earthquake control at Rangely, Colorado. *Science* (191), 1230-1237.

Rutqvist, J. B. (2008). Coupled reservoir-geomechanical analysis of the potential for tensile and shear failure associated with CO2 injection in multilayered reservoir-caprock systems. *Inernational Journal of Rock Mechanics & Mining Sciences , 45*, 132-143.

Segall, P. F. (1998). A note on induced stress changes in hydrocarbon and geothermal reservoirs. *Tectonophysics , 289*, 117-128.

Soltanzadeh, H. H. (2008). Semi-analytical models for stress change and fault reactivation induced by reservir production and injection. *Journal of Petroleum Science & Engineering , 60*, 71-85.

Soltanzadeh, H. H. (2008). Semi-analytical models for stress change and fault reactivation induced by reservoir production and injection. *Journal of Petroleum Science & Engineering , 60*, 71-85.

Sun, H. F. (2008). New equations for density, entropy, heat capacity and potential temperature of a saline thermal fluid. *ScienceDirect: Deep-Sea Research 1 , 55*, 1304-1310.

Suri, A. S. (2010). A Simple and Accurate Model for Well Productivity for Hydraulically Fractured Wells . *SPE Production & Engineering* , 453-460.

Theis, C. (1935). The relation between the lowering of the Piezometric surface and the rate and duration of discharge of a well using ground-water storage. *Eos Trans. Am. Geophys. Union , 16*, 519-524.

TNO, P. E. (2014). *Literature review on Injection-Related Induced Seismicity and its relevance to Nitrogen Injection.* Utrecht: TNO.

Van den Broek, J. (2015). *Well Stimulation.* Arnhem: IF Technology.

van Everdingen, E. (1953). The skin effect and its influence in the productive capacity of a well. *AIME , 198*, 171-176.

Van Wees, J. B.-V. (2014). Geomechanics Response and Induced Seismicity during Gas Field Depletion in the Netherlands. *Geothermics , 52*, 206-219.

van Wees, J. K. (2012). Geothermal aquifer performance assessment for direct heat production - Methodology and application to Rotliegend aquifers. *Netherlands Journal of Geosciences , 91* (4), 654-665.

Veldkamp, J. L. (2015). *Thermal fracturing due to low injection temperatures in geothermal doublets.* Utrecht: TNO.

Veldkamp, J. P. (2015). *DoubletCalc 2D 1.0 User Manual.* Utrecht : TNO .

Wang, H. (2016). Poro-elasto-plastic modeling of complex hydraulic fracture propagation; simulations multi-fracturing and producing well inteference. *Acta Mech , 227*, 507-525.

Zoback, M. (2007). *Reservoir Geomechanics .* Cambridge University Press. .

APPENDIX A

List of Symbols

Symbol	Parameter	Unit
a	Major axis of an ellips	m
A	Cross-sectional area of a fracture	m^2
α	Biot's coefficient	-
$α_{cap}$	Thermal diffusivity of cap/base rock	m^2/s
b	Minor axis of an ellips	m
β	Linear thermal expansion coefficient	$°C^{-1}$
B_v	Volumetric thermal expansion coefficient	$3*β$
c_{gr}	Compressibility of grains in the reservoir	Pa^{-1}
c_t	Total reservoir compressibility	Pa^{-1}
C	Heat Capacity	$J/m^3°C$
Cc	Leak off component (viscosity vs reservoir compressibility)	-
C_L	Leak-off coefficient	-
C_m	Coefficient of uniaxial compaction	-
C_v	Leak off component (viscosity vs permeability)	-
C_w	Leak off component (Wall building)	-
CFS	Coulomb Failure Stress	Pa
$δ_{ij}$	Kronecker Delta	-
Δh	Vertical displacement of the reservoir; either thermal ($Δh^T$) or poro-elastic ($Δh^P$)	m
ΔP	Pressure change	Pa
$Δσ^P$	Poro-elastic stress change	Pa
$Δσ^T$	Thermo-elastic stress change	Pa
ΔT	Temperature change	°C
e	Ratio of minor & major axis of an ellips	-
E	Young's modulus	Pa
φ	Porosity	-
g	Gravitational acceleration	m/s^2
$γ_a$	Stress arching ratio	-
$γ_P$	Poro-elastic stress path ratio	-
h	Thickness of reservoir	m
J	Linear coefficient of pore pressure expansion/productivity index	$[Pa^{-1}]$/ [STB/day/psi]
J_0	Base productivity index	STB/day/psi
k	Permeability	D
K	Bulk modulus (s = solid, fr = drained)	Pa
K_f	Effective fracturing fluid filtrate permeability	D
λ	Euler-Macharoni constant (=0.5772156649)	-
L	Well distance	m
L_f	Fracture half-length	m
μ	Viscosity	Pa.s
$μ_f$	Internal friction coefficient	-
M_w	Earthquake moment magnitude	-

GEO CAP

P	Pressure	Pa
Pe	Peclet number	-
P_f	Pore fluid pressure	Pa
q	Angle between effective principal stresses	°
Q	Volumetric injection rate	m^3/d
Q_m	Mass flow rate	kg/d
r	Distance from well (radial)	m
r_{well}	Outer well radius	m
ρ	Density	Kg/m3
Rc	Radius of cooled front	m
R_{ntg}	Net to gross ratio	-
R_{res}	Radial extent of the reservoir (until boundary)	m
s	Well drawdown	m
σ	Stress (1,2,3 for principal stresses, v,h,H for vertical, minimum horizontal and maximum horizontal stress)	Pa
σ'	Effective stress	Pa
$σ_n$	Normal stress	Pa
$σ_{ten}$	Tensile strength	Pa
S_o	Cohesion strength of rock	Pa
S	Storativity	-
Skin	Skin factor of well	-
t	Injection time	d
τ	Shear stress	Pa
$τ_c$	Critical shear stress	Pa
θ	Fault dip w.r.t. the $σ_1$ direction	°
T	Temperature	°C
T_r	Transmissivity	m^2/d
TDS	Total dissolved solids (solinity)	Kg/L
u_h	Horizontal displacement	m
u_v	Vertical displacement	m
N	Poisson's ratio	-
V	Volume	m^3
w	Fracture width	m
w_{av}	Average fracture width	m
z	Depth	m

Subscripts

BH	Borehole
c	Cooled
D	Dimensionless coefficient/parameter
fl	Flooded
frac	Fracture
Inj/w	Injective/water
Init	Initial
l	Lithos (rock)
res	Reservoir
skin	Skin factor
Tip	Fracture tip

APPENDIX B

Doublet Calc Simulation

Geotechnics (Input)

Property	min	median	max
aquifer permeability (mD)	150.0	250.0	500.0
aquifer net to gross (-)	0.75	0.8	0.85
aquifer gross thickness (m)	95.0	105.0	115.0
aquifer top at producer (m TVD)	2255.0	2505.0	2756.0
aquifer top at injector (m TVD)	2221.0	2468.0	2715.0
aquifer water salinity (ppm)	100000.0	120000.0	140000.0

Property	value
number of simulation runs (-)	1000.0
aquifer kh/kv ratio (-)	1.0
surface temperature (°C)	10.0
geothermal gradient (°C/m)	0.031
mid aquifer temperature producer (°C)]	0.0
inital aquifer pressure at producer (bar)]	0.0
[initial aquifer pressure at injector (bar)]	0.0
exit temperature heat exchanger (°C)	35.0
distance wells at aquifer level (m)	1460.0
pump system efficiency (-)	0.61
production pump depth (m)	500.0
pump pressure difference (bar)	40.0
outer diameter producer (inch)	6.13
skin producer (-)	0.0
skin due to penetration angle p (-)	-0.97
pipe segment sections p (m AH)	500.0,1054.0,1930.0,2678.0
pipe segment depth p (m TVD)	500.0,1054.0,1833.0,2505.0
pipe inner diameter p (inch)	5.0,12.38,8.62,6.62
pipe roughness p (milli-inch)	1.2,1.2,1.2,1.2
outer diameter injector (inch)	6.13
skin injector (-)	0.0
skin due to penetration angle i (-)	-0.97
pipe segment sections i (m AH)	50.0,1054.0,1930.0,2645.0
pipe segment depth i (m TVD)	50.0,1054.0,1833.0,2468.0
pipe inner diameter i (inch)	5.0,12.38,8.62,6.62
pipe roughness i (milli-inch)	1.2,1.2,1.2,1.2

Geotechnics (Output)

Monte Carlo cases (stochastic inputs)	P90	P50	P10
aquifer kH net (Dm)	16.25	21.46	33.09
mass flow (kg/s)	35.22	43.57	58.45
pump volume flow (m³/h)	119.8	148.6	198.6
required pump power (kW)	218.2	270.7	361.8
geothermal power (MW)	6.42	8.27	11.25
COP (kW/kW)	28.0	30.4	32.9
aquifer pressure at producer (bar)	240.29	254.94	270.42
aquifer pressure at injector (bar)	237.34	251.01	265.6
pressure difference at producer (bar)	11.89	13.71	14.61
pressure difference at injector (bar)	22.36	25.65	27.37
aquifer temperature at producer * (°C)	85.0	89.27	93.56
temperature at heat exchanger (°C)	82.42	86.51	90.67

base case (median value inputs)	value
aquifer kH net (Dm)	21.0
mass flow (kg/s)	43.05
pump volume flow (m³/h)	146.6
required pump power (kW)	267.1
geothermal power (MW)	8.12
COP (kW/kW)	30.4
aquifer pressure at producer (bar)	255.08
aquifer pressure at injector (bar)	251.18
pressure difference at producer (bar)	13.78
pressure difference at injector (bar)	25.81
aquifer temperature at producer * (°C)	89.28
temperature at heat exchanger (°C)	86.51
pressure at heat exchanger (bar)	16.35

* @ mid aquifer depth

Figuur 34: *Input for Doublet Calc simulation for different Skin factors. Results are shown in section* XXX

APPENDIX C

User Guide for Tools

The tools described above are made in three different Matlab Programs. They give quick calculations and are easy to use.

1. Hydrothermal Fracturing Tool (1D) – chapter **Fout! Verwijzingsbron niet gevonden.**

2. Compaction and Subsidence Tool (1D) – chapter **Fout! Verwijzingsbron niet gevonden.**

3. Induced Stresses and Failure Tool (1D or 2D) – chapter **Fout! Verwijzingsbron niet gevonden.**

All calculations that are used in the models are described in the chapters linked to the tool.

Stresses and Failure Tool

This tool determines the evolution of stress changes around the wellbore as a result of cold fluid injection. The stress changes are used to determine potential reservoir compaction, tensile failure around the wellbore or shear failure. To use it, one only has to click on the run button and define the input parameters and choose your type of output

Input

The input is collected by a bunch of dialog boxes. The input parameters that have to be defined are given in **Fout! Verwijzingsbron niet gevonden.**, together with their default value.

Input

The input is collected by a bunch of dialog boxes. The input parameters that have to be defined are given in **Fout! Verwijzingsbron niet gevonden.**, together with their default value.

Input Parameters				
Parameter	**Unit**	**Default value**		
		ISFT	CST	HFT
X-coordinates	-	-1000-1000	-	-
Y-coordinates	-	-500-500	-	-
Coordinates of the well	-	(0,0)	-	-
Radius of well	m	0.11	0.11	0.11
Reservoir Properties				
Reservoir depth (Top/Bottom)	m	3550	2000	
Reservoir thickness	m	200	100	
Reservoir temperature	°C	120	85	
Permeability	mD	29	200	
Porosity	-	0.16	0.20	
Density of rock	kg/m^3	2300	2700	
Formation compressibility	Pa^{-1}	4e-7	4e-7	
Thermo-elastic expansion coefficient	-	1e-5	2e-5	
Heat capacity of reservoir	J/(m^3 °C)	2.0e6	2.1e6	

Young's modulus	GPa	15	9	
Poisson's ratio	-	0.25	0.35	
Biot's coefficient	-	1	1	
Cap/Base rock properties				
Heat capacity of cap/base rock	J/(m^3 °C)	2.1e6	2.1e6	
Thermal diffissivity	m^2/s	1.3e-6	1.3e-6	
Injection & Simulation Properties				
Injection temperature	°C	35	30	
Injection rate	m^3/d	4800	4800	
Salinity/Total dissolved solids	g/L	200	70	
Compressibility of injectate	Pa^{-1}	4.4e-10	4.4e-10	
Time of injection	Yrs	35	5	
Time step	Yrs	1	1	

***Table 6**: Default values for the Induced Stresses and Failure tool (ISFT), the Compaction and Subsidence tool (CST), and the Hydrothrmal Fracking tool (HFT).*

You can either choose if you want to define the initial stress and pressure manually or if they should be calculated by equation XX and XX. These equations give the hydrotstatic pressure at depth and the lithostatic stress of the overburden. This is then used to define the minimum horizontal stress (Eq. XX)

Output

This model can be used for three different applications. In the dialog box in **Fout! Verwijzingsbron niet gevonden.** , one can define in which output values he or she is interested.
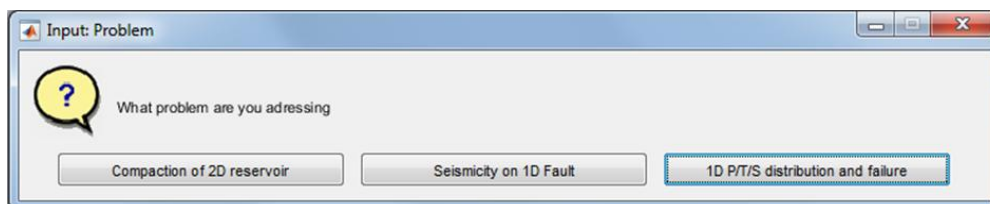

***Figure 35**: Dialog box to define which output one wants.*

The default choice, **the 1D P/T/S distribution and failure,** calculates the temperature and pressure distributions around the wellbore and the associated poro- and thermo elastic stress changes. These stress changes are thereafter used to define the evolution of the tensile strength of the rock, the effective minimum horizontal stress and the effective overburden stress. In a normal faulting regime, as is applicable for a large part of the Netherlands, these stresses can then be used to determine the potential for failure. The left bottom plot in **Fout! Verwijzingsbron niet gevonden.** shows the area around the well bore that is prone to tensile failure, or in other words the opening of thermo-hydraulic fractures. This is the case for a critical tensile failure criterion (CFT) larger than 0, which is defined as the total pore fluid pressure minus the tensile rock strength at each location. The bottom right plot in **Fout! Verwijzingsbron niet gevonden.** shows the area around the wellbore that is prone to shear failure. In this case we assume pre-existing faults with a pre-defined internal friction coefficient and dip, and a prefect orientation with respect to the minimum horizontal stress. Faults in this area are prone to fail when the critical shear failure criterion is larger than 0.
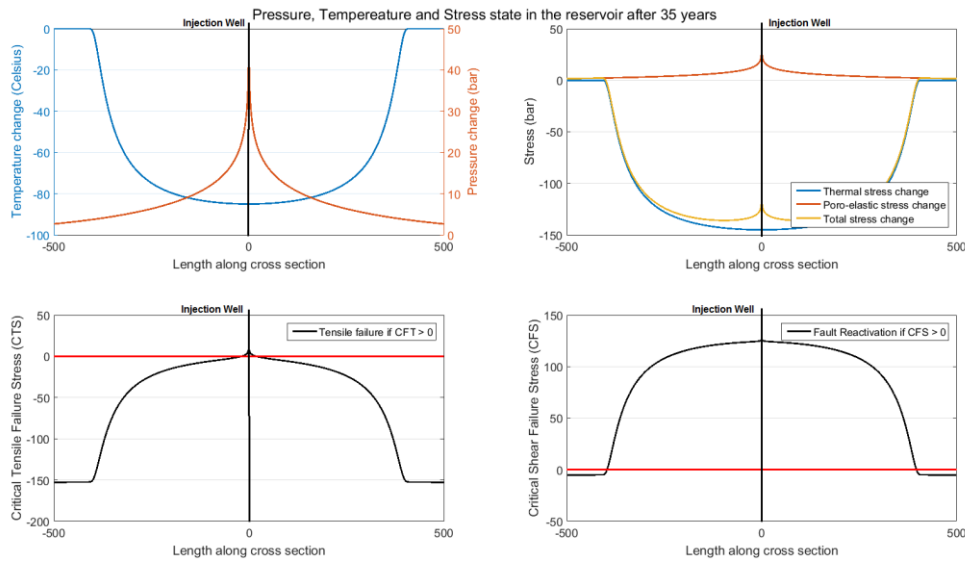
Figure 36: Output plots for the 1D P/T/S distribution and failure application

The other seismicity choice, **Seismicity on a 1D fault**, determines the potential on shear failure on a fault crosscutting the reservoir. The fault can be chosen by defining the X-, and Y- coordinates of each fault point (**Fout! Verwijzingsbron niet gevonden.**). Then for each fault point the stress evolution is calculated, and the associated effective normal stress and effective shear stress. These stress paths are plotted in the Mohr Coulomb concept (right plot in **Fout! Verwijzingsbron niet gevonden.**). Whenever a stress path crosses the failure criterion line, this point on the fault will fail in shear. The stress paths all first show a shift of the stress path to the left, with a little decrease in absolute shear stress. This is the effect of the pressure front travelling through the fault. And fracture points close to the well are thereafter affected by the temperature front travelling through, which results in an decrease in stress path, but an increase in absolute shear stress.
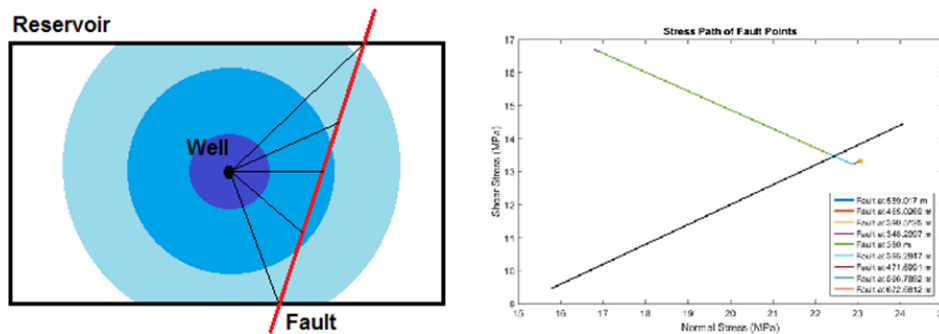

Figure 37: Output plots for the seismicity on a 1D fault application. Left) Concept of arbitrary fault in a reservoir. Points on the fault have different distances w.r.t the well. Right) Stress path evolution of fault points. Fault points in the flooded area move further away from the failure line, while faults affected by temperature changes are prone to fail.

The last application, compaction of the 2D reservoir, gives the temperature, pressure and stress changes of each point in a chosen reservoir. It also defines the area around the well that is prone to tensile failure. The application assumed that no fractures are formed during injection and thus the distribution of T and P is radial around the wellbore. Thereafter, the thermal and poro-elastic compaction at the reservoir level can be calculated and the compaction bowl within the reservoir is plotted as you see in **Fout! Verwijzingsbron niet gevonden.**.
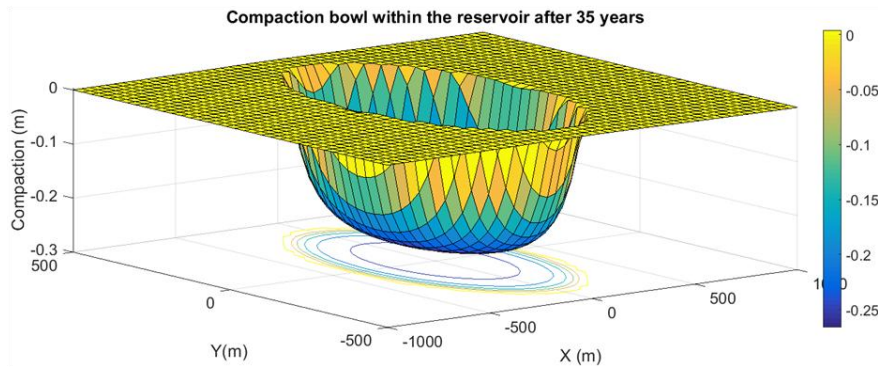
Figure 38: *Output plots for the compaction of the 2D reservoir application.*

Compaction and Subsidence

The compaction and subsidence tool can be used to define how cold fluid injection affects the reservoir and leads to compaction. It is also capable of translating the compaction in depth to a subsidence profile at the surface. Basically, the lay-out of the tool is the same as the stresses and failure tool. Input is collected by various dialog boxes or through a text file and the default values are listed in table XX. And again, the stresses can be either defined as a result of burial depth or manually. One can now also choose to use the formation fluid application or to ignore the temperature, pressure and salinity effect on fluid characteristics.

Output

Figure 41 and **42** present the results of the compaction and subsidence tool. The tool provides the combined temperature, pressure and stress around the wellbore for various time steps during injection. These changes are translated to compaction at the reservoir by the concept of plane strain. In other words, these stresses are assumed to only cause displacement in the vertical direction. The compaction then results in horizontal and vertical displacement at the surface level. This is calculated by Geertsma (1973), as is described in more detail in chapter 4. The figures show that the pressure effects are largest in the vicinity of the well. The temperature front travels through the reservoir in time and has more effect on the stress changes in these areas. This results in a larger compaction due to temperature changes than in uplift due to an increased pressure. At the surface level, the vertical movement is highest right above and around the injection well. Further away from the well, part of the stress changes is accommodated by horizontal displacement towards the well on order to fill up the "voids". There is a point for which the horizontal displacement becomes larger than the vertical displacement.

Hydrothermal Fracturing Tool

The hydrothermal fracturing tool can be used to define the effects of induced stresses, due to injection, on the formation and growth of fractures. This is used during reservoir stimulation and can be used to improve the productivity of the well, by decreasing the flow resistance into the reservoir. Similar to the models named above, this tool collects input parameters from several dialog boxes. Then three various methods can be selected to determine the fracture geometry in time; an iterative method, the PKN method and a method by Koning (section **Fout! Verwijzingsbron niet gevonden.**).
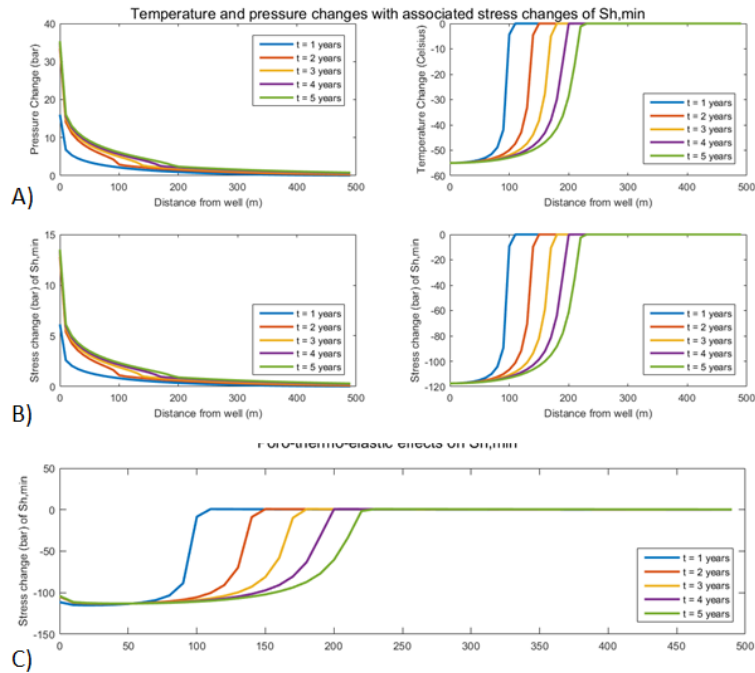
Figure 39: Induced pressure and temperature effects around a wellbore. A) The pressure and temperature difference as a result of injection. B) shows the accommodating stress changes due to poro-elastic effects (left) and thermos-elastic effects (right). C) The combined stress changes of B.
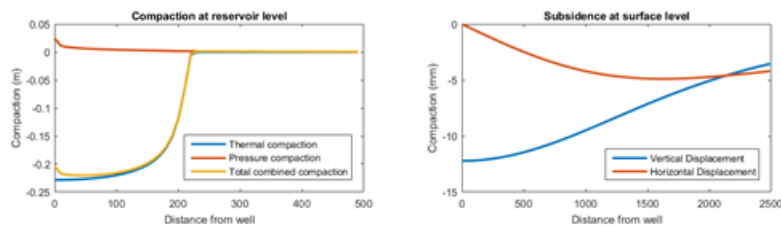

Figure 40: (Left) Compaction in the reservoir as a result of pressure and temperature changes. (Right) The associated subsidence at the surface level.

Output

Figure 43 and **44** show the output of an arbitrary fracture model. The input is similar to the ones used in chapter 3 and the iterative fracture growth approximation is used. The tool provides and first order approximation on the size and geometry of the fracture and the result in shape of the leak-off field. As the fracture grows in time, the cooled and flooded front around the fracture starts to take develop elliptically. **Figure 43B** shows that the net pressure at the fracture tip is always cannot become positive; the pressure at the tip must always be smaller than the tensile strength. If not, the fracture will grow. The half-length of the fracture is proportional to the square root of time. **Figure 43D** represents the evolution of fracture width and the corresponding volume of the fracture.
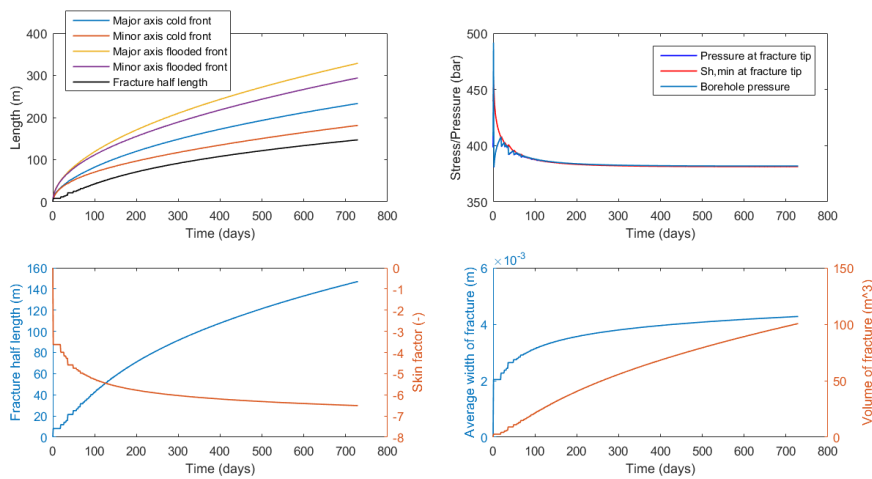
Figure 23: *The evolution of a hydrothermal fracture A) Fracture growth and the extend of the cooled and flooded front in time. B) The pressure and tensile strength at the tip of the fracture. C) The Skin with time and fracture length. D) The width and volume growth of the induced fracture*
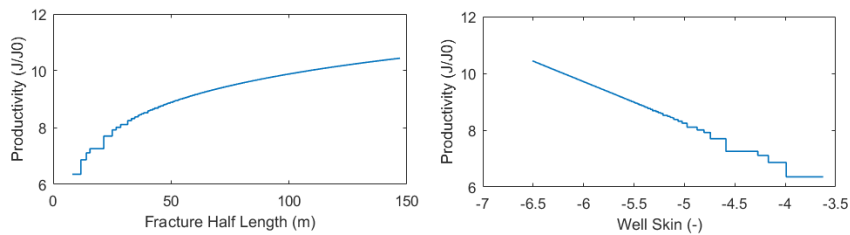

Figure 42: *The well productivity as a result of fracturing. Left) The productivity w.r.t. the fracture half-length and (right) w.r.t. the well skin. The productivity of the well increases if J/J0 > 1. Note that the productivity index and the skin are linearly related.*

As stated in section 3.3.8, the productivity of the well will increase as the fracture grows. The productivity index, as shown in Figure 44, is a measurement of the well productivity compared to an unstimulated well. The well is more efficient for productivities higher than 1. This is linearly related to the skin of the well and logarithmically to the extent of the fracture.